

# The Diverse Broad Band Lightcurves of Swift GRBs Reproduced With The Cannonball Model

Shlomo Dado<sup>1</sup>, Arnon Dar<sup>2</sup>

## ABSTRACT

Two radiation mechanisms, inverse Compton scattering (ICS) and synchrotron radiation (SR), suffice within the cannonball (CB) model of long gamma ray bursts (LGRBs) and X-ray flashes (XRFs) to provide a very simple and accurate description of their observed prompt emission and afterglows. Simple as they are, the two mechanisms and the burst environment generate the rich structure of the light curves at all frequencies and times. This is demonstrated for 33 selected Swift LGRBs and XRFs, which are well sampled from early time until late time and well represent the entire diversity of the broad band light curves of Swift LGRBs and XRFs. Their prompt gamma-ray and X-ray emission is dominated by ICS of glory light. During their fast decline phase, ICS is taken over by SR which dominates their broad band afterglow. The pulse shape and spectral evolution of the gamma-ray peaks and the early-time X-ray flares, and even the delayed optical ‘humps’ in XRFs, are correctly predicted. The canonical and non-canonical X-ray light curves and the chromatic behaviour of the broad band afterglows are well reproduced. In particular, in ‘canonical’ X-ray light curves, the initial fast decline and rapid softening of the prompt emission, the transition to the plateau phase, the subsequent gradual steepening of the plateau to an asymptotic power-law decay, and the transition from chromatic to achromatic behaviour of the light-curves agree well with those predicted by the CB model. The Swift early-time data on XRF 060218 are inconsistent with a black body emission from a shock break-out through a stellar envelope. Instead, they are well described by ICS of glory light by a jet breaking out from SN2006aj. The start time of the X-ray emission does not constrain the exact time of the core’s collapse before the launch of the jet, nor does it constrain possible ejections of additional CBs farther off axis.

---

<sup>1</sup>dado@phep3.technion.ac.il, Physics Department, Technion, Haifa 32000, Israel

<sup>2</sup> arnon@physics.technion.ac.il, Physics Department, Technion, Haifa 32000, Israel  
dar@cern.ch, Theory Unit, CERN,1211 Geneva 23, Switzerland

## 1. Introduction

Since the launch of the Swift satellite, precise data from its Burst Alert Telescope (BAT) and X-Ray Telescope (XRT) have been obtained on the spectral and temporal behaviour of the X-ray emission of long-duration  $\gamma$ -ray bursts (LGRBs) and X-ray flashes (XRFs) from their beginning until late times. The early data are often complemented by the ultraviolet-optical telescope (UVOT) on board Swift, and by ground-based UVO and NIR robotic and conventional telescopes. The ensemble of these data have already been used to test the most-studied theories of long duration GRBs and their afterglows (AGs), the *Fireball* (FB) models (see, e.g., Zhang & Mészáros 2004, Zhang 2007, and references therein) and the *Cannonball* (CB) model [see, e.g., Dar & De Rújula 2004 (hereafter DD2004), Dado, Dar & De Rújula (hereafter DDD) 2002a, 2003a, and references therein].

The Swift X-ray light curves of LGRBs roughly divide into two classes, ‘canonical’ and non canonical (Nousek et al. 2006, O’Brien et al. 2006, Zhang 2007). When measured early enough, the observed X-ray emission has prompt peaks which coincide with the  $\gamma$ -ray peaks of the GRB, and a rapidly declining light curve with a fast spectral softening after the last detectable peak of the GRB. This rapid decline and spectral softening of the prompt emission end within a couple of hundreds of seconds. In ‘canonical, LGRBs the X-ray light curve turns sharply into a much flatter ‘plateau’ with a much harder power-law spectrum, typically lasting thousands to tens of thousands of seconds, and within a time of order one day it steepens into a power-law decay, which lasts until the X-ray AG becomes too dim to be detected (Fig. 1).

The plateau phase is missing in non canonical GRBs, and the asymptotic power-law decline begins during the decline of the prompt emission and lasts until the X-ray become too dim to be detected (Fig. 2) without any observable break.

In a significant fraction of canonical GRBs, the rapid decay and fast spectral softening of the prompt emission first changes to a slower power-law decay,  $\sim t^{-2.1}$ , with a harder spectrum before it reaches the plateau phase (Fig. 3). We shall refer to such light curves as ‘semi canonical’.

The Swift X-ray data show a flaring activity in a large fraction of GRBs. both at early and late times. The X-ray peaks during the prompt  $\gamma$ - ray emission follow the pattern of the  $\gamma$ -ray pulses, they must have a common origin. In many GRBs, superimposed on the early-time fast decaying X-ray light curve, there are X-ray flares, whose peak intensities also decrease with time and whose accompanying  $\gamma$ -ray emission is probably below the detection sensitivity of BAT. Yet, their spectral and temporal behaviour is similar to that of the prompt X/ $\gamma$  pulses. Very often the flaring activity continues into the afterglow phase. However late-

time flares seem to exhibit temporal and spectral behaviours different than those of the early-time flares.

Neither the general trend, nor the frequently complex structure of the Swift X-ray data were predicted by (or can be easily accommodated within) the standard FB models (see, e.g., Zhang & Mészáros 2004, Piran 2005, for reviews). Much earlier confrontations between predictions of the FB models and the observations also provided severe contradictions, such as the failure to understand the prompt spectrum on grounds of synchrotron radiation (e.g., Ghisellini, Celotti, & Lazzati 2000), or the ‘energy crisis’ in the comparison of the bolometric prompt and AG fluences (e.g., Piran 1999, 2000). We have discussed elsewhere other problems of FB models (DD2004, Dar 2005 and references therein), including those related to ‘jet breaks’ (e.g., DDD2002a, Dar 2005, DDD2006), and the a-posteriori explanations of the reported detections of large  $\gamma$ -ray polarization (DDD2007b, and references therein).

The Swift data have challenged the prevailing views on GRBs. Kumar et al. (2007) concluded that the prompt  $\gamma$ -ray emission cannot be produced in shocks, internal or external. Zhang, Liang & Zhang 2007 found that the fast decay and rapid spectral softening ending the prompt emission cannot be explained by high latitude emission. The X-ray and optical afterglows of Swift GRBs are very chromatic at early time in contrast with the fireball model expectation. Moreover, Curran et al. (2006) have carefully examined Swift data and found that X-ray and optical AGs have achromatic breaks which differ significantly from the jet break of the blast wave model of AGs. Burrows and Racusin (2007) examined the XRT light curves of the first  $\sim 150$  Swift GRBs and reported that the expected jet breaks are extremely rare. In particular, Liang et al. (2008) have analyzed the Swift X-ray data for the 179 GRBs detected between January 2005 and January 2007 and the optical AGs of 57 pre- and post-Swift GRBs. They found that not a single burst satisfies all the criteria of a jet break.

In spite of the above failures, not all authors are so critical. Some posit that the Swift data require only some modifications of the standard FB models in order to accommodate the results (e.g., Panaitescu et al. 2006, Dai et al. 2007, Sato et al. 2007). Others still view the situation with faith (e.g., Covino et al. 2006, Dai et al 2008, Racusin et al. 2008a).

The situation concerning the CB model is different. The model was based on the assumption that LGRBs are produced by highly relativistic jets of plasmoids of ordinary matter (Shaviv & Dar 1995) ejected in core-collapse supernova (SN) explosions akin to SN1998bw (Dar & Plaga 1999, Dar & De Rújula 2000). It successfully described the broadband AGs observed before the Swift era ( e.g., DDD2002a, DDD2003a) and exposed the consistent photometric evidence for a LGRB/SN association in all nearby GRBs (DDD2002a, DD2004 and references therein) long before GRB 030329. In the case of GRB 030329 the

first  $\sim 6$  days of AG data were described by the CB model precisely enough to extrapolate them to predict even the date in which its associated SN would be bright enough to be observed (DDD2003c). General acceptance of the GRB-SN association waited until the spectroscopic discovery of an SN2003dh coincident with GRB 030329 (Hjorth et al. 2003, Stanek et al. 2003) and until additional discoveries of spectroscopically proven GRB-SN associations such as GRB030213/SN2003lw (Malesani et al. 2003), GRB021211/SN2002lt (Della Valle et al. 2003), XRF060218/SN2006aj (Campana et al. 2006b, Pian et al. 2006, Mazzali et al. 2006) and XRF080109/SN2008D (Malesani et al. 2008, Modjaz et al. 2008).

The CB model (DD2004) has been applied successfully to explain all the main observed properties of long GRBs and XRFs before the Swift era. (see. e.g., Dar 2005 and references therein). The model is summarized in §2. For more detailed summaries, see, e.g., De Rújula, 2007a,b.

In this report we extend and refine our analysis of the temporal and spectral behaviour of the  $\gamma$ -ray, X-ray and optical light curves of GRBs during the prompt emission and its rapid decay phase, and the afterglow phase. The observed prompt spectrum in the  $\gamma$ -ray to X-ray domain is that predicted for the prompt emission (DD2004), which in the CB model is Compton-dominated. The observed widths of the  $\gamma$ -ray and X-ray peaks, as well as lag-times between them and their relative fluences, are in accordance with the model’s predictions, if free-free absorption dominates the transparency of the CBs to eV photons in the CBs’ rest frame. This prompts us to investigate whether or not the CB model can be further simplified, to describe the data in terms of only two emission mechanisms, inverse Compton scattering and synchrotron radiation. We shall see that this simple picture, explicitly based on the predictions in DDD2002a and DD2004, gives a straight-forward and successful description of the Swift GRB data, at all observed energies and times.

In the CB model which is summarized in §2 inverse Compton scattering (ICS) of glory photons is the origin of the prompt  $\gamma$ /X-ray peaks, as we review in §3. Each peak is generated by a cannonball emitted by the ‘engine’, the accreting compact object resulting from a core-collapse supernova event. We shall see that ICS correctly describes the prompt peaks, extending even into the optical domain in XRFs in which the relevant observations are available, such as in XRF 060218. The natural explanation of the early time flares is the same as that of the stronger flares: ICS of glory photons by the electrons of CBs ejected in late accretion episodes of fall-back matter on the newly formed central object. These CB emissions must correspond to a weakening activity of the engine, as the accreting material becomes scarcer.

In the CB model, from the onset of the ‘plateau’ onwards, the X-ray, optical (DDD2002a) and radio (DDD2003a) afterglows are dominated by synchrotron radiation (SR), the CB-

model predictions for which are reviewed in §4. On occasion these AGs also have transient rebrightenings (‘very late’ flares), two notable cases before the Swift era being GRB 970508 (Amati et al. 1999, Galama et al. 1998a) and GRB 030329 (Lipkin et al. 2004). During these episodes, the spectrum continues to coincide with the one predicted on the basis of the synchrotron mechanism that dominates the late AGs. These very late flares are well described by encounters of CBs with density inhomogeneities in the interstellar medium (DDD2002a, DD2004). Very late flares in the XUVONIR afterglow may have this origin as well.

In this report we compare the predictions of the CB model and the observed X-ray and optical light curves of 33 selected GRBs, which are well sampled from very early time until late time, have a relatively long follow up with good statistics and represent well the entire diversity of Swift GRBs. These include the brightest of the Swift GRBs (080319B), the GRB with the longest measured X-ray emission (060729), a couple with canonical X-ray light curves (050315, 060526, 061121 and 080320) with, and without superimposed X-ray flares, GRBs with semi-canonical light curves (060211A, 061110A, 070220, 08033, 080307, 051021B) and non-canonical light curves (061007, 061126, 060206), and some of the allegedly most peculiar GRBs (050319, 050820A, 060418, 060607A, 070101A, 061126). We also compare the CB model prediction and the observed X-ray light curve of additional 12 GRBs with the most rapid late-time temporal decay.

In the CB model, LGRBs and XRFs are one and the same (DD2004, Dado et al. 2004c) –the general distinction being that XRFs are viewed at a larger angle relative to the direction of the approaching jet of CBs or have a relatively small Lorentz factor. Thus we include a Swift XRF of particular interest in our analysis: 060218. Its X-ray light curve is shown to be the normal X-ray light curve of a GRB viewed far off axis, and not the emission from the break out of a spherical shock wave through the stellar envelope. Its optical AG, at various frequencies, shows not only the light curves and spectra of its associated supernova, but a series of broad peaks between 30 ks and 60 ks after trigger which are interpreted as the optical counterparts of the sole prompt X-ray peak of this XRF. The expressions describing an ICS-generated peak at all frequencies allow us to predict the positions and magnitudes and pulse shape of these broad peaks a gigantic extrapolation in time, radiated energy and frequency.

After submitting for publication a first version of a comprehensive comparison between the CB model predictions and Swift observations (DDD2007c), we have compared many more Swift data with the CB model predictions in order to further test its ability to predict correctly all the main observed properties of GRB light curves. These included the rapid spectral evolution observed during the fast decay of the prompt emission in ‘canonical’ GRBs

(DDD2008a), and the ‘missing AG breaks’ in the AG of several GRBs (DDD2008b). We have also extended the CB model to describe short hard bursts (SHBs) and confronted it with the entire data on all SHBs with well measured X-ray and/or optical afterglows (Dado & Dar 2008a).

Together with the GRBs discussed in this report, by now we have analyzed and published CB model fits to the light curves of more than 100 LGRBs and SHBs. The CB model continued to be completely successful in comparison of its predictions with the data.

## 2. The CB Model

In the CB model (e.g., DD2004 and references therein) *long-duration* GRBs and their AGs are produced by bipolar jets of CBs which are ejected (Shaviv & Dar, 1995, Dar & Plaga 1999) in *ordinary core-collapse* supernova explosions<sup>1</sup>. An accretion disk or a torus is hypothesized to be produced around the newly formed compact object, either by stellar material originally close to the surface of the imploding core and left behind by the explosion-generating outgoing shock, or by more distant stellar matter falling back after its passage (De Rújula 1987). As observed in microquasars (e.g., Mirabel & Rodriguez 1999, Rodriguez & Mirabel 1999 and references therein), each time part of the accretion disk falls abruptly onto the compact object, a pair of CBs made of *ordinary-matter plasma* with a typical baryonic number,  $N_B \sim 10^{50}$ , are emitted with large bulk-motion Lorentz factors, typically  $\gamma_0 \sim 10^3$ , in opposite directions along the rotation axis, wherefrom matter has already fallen back onto the compact object, due to lack of rotational support.

The  $\gamma$ -rays of a single pulse of a GRB are produced as a CB coasts through the SN *glory* – the progenitor’s pre-supernova light, the SN light and the collimated CB light, scattered by the ‘wind’: the ejecta puffed by the progenitor star continuously or in a succession of pre-SN flares. The electrons enclosed in the CB Compton up-scatter the photons of the glory to GRB energies. The initial fast expansion of the CBs and the increasing transparency of the wind environment as the CBs penetrates it, result in the fast rise of GRB pulses. As the CB coasts further through the SN glory, the density and temperature decreases rapidly. Consequently,

---

<sup>1</sup>Supernovae associated with GRBs are viewed uncommonly close to their CB jet axis, near which the non-relativistic SN ejecta are faster than average. Their observed large velocities may, erroneously in our view, lead to their interpretation of the SNe as a very special GRB-associated class of ‘*hypernovae*’. Moreover, the observed velocities of the ejecta of ‘hypernova’ a year or two after the explosion, i.e., before they swept a significant mass of circumburst matter, are typically 5000-7000 km/s, corresponding to a normal kinetic energy release of  $2.5\text{-}5 \times 10^{51}$  erg in SNIb/c.

the energy of the up-scattered photons is continuously shifted to lower energies and their number decreases rapidly. Typically, the ensuing fast decline of the prompt emission is taken over, within a couple of minutes of observer’s time, by a broad-band synchrotron emission from swept-in electrons from the wind and the interstellar medium (ISM) spiraling in the CB’s enclosed magnetic field.

In the CB model there is no clear-cut *temporal* distinction between prompt and *afterglow* signals. There are, however, two rather distinct radiation mechanisms: inverse Compton scattering and synchrotron radiation. For all cases we have studied, the prompt emission of  $\gamma$ -rays, X-rays and optical light in XRFs is dominated by ICS whereas in ordinary GRBs, the prompt emission of  $\gamma$  and X-rays is dominated by ICS and SR dominates the prompt optical emission and the broad band afterglow emission. Usually, the SR takes over the X-ray emission during the fast decay of the prompt emission or at the onset of the ‘plateau’ phase. Late flares seem to be dominated by SR.

### 3. Inverse Compton Scattering

#### 3.1. The spectrum of ICS pulses

During the initial phase of  $\gamma$ -ray emission in a GRB, the Lorentz factor  $\gamma$  of a CB stays put at its initial value  $\gamma_0 = \mathcal{O}(10^3)$ , for the deceleration induced by the collisions with the ISM has not yet had a significant effect (DDD2002a, DDD2003a). Let  $\theta$  be the observer’s angle relative to the direction of motion of a CB. The Doppler factor by which light emitted by a CB is boosted in energy is,

$$\delta = \frac{1}{\gamma(1 - \beta \cos \theta)} \approx \frac{2\gamma}{(1 + \gamma^2 \theta^2)}, \quad (1)$$

where the approximation is excellent for  $\gamma \gg 1$  and  $\theta \ll 1$ . The emitted light is forward-collimated into a cone of characteristic opening angle  $1/\gamma$ , so that the boosted energetic radiation is observable for  $\theta = \mathcal{O}(1/\gamma_0)$ . This implies that the typical initial Doppler factor of a GRB is:  $\delta_0 = \mathcal{O}(10^3)$ .

The burst environment is very complicated, and can be estimated only very roughly: After ejection the fast expanding CB propagates through a cavity, which was produced by the pre-supernova ejecta/wind, and shortly encounters the much slower wind which has roughly a density distribution of the form,  $n(r) \propto 1/r^2$ . The initially fast expanding CB scatters the quasi spherical light scattered/emitted by the wind, which was shined before by the

progenitor star, the SN and the collimated light from the CB itself<sup>2</sup>. This quasi spherical glory light has a thin thermal bremsstrahlung spectrum,

$$\epsilon \frac{dn_\gamma}{d\epsilon} \approx n_\gamma(r) \left( \frac{\epsilon}{T_g} \right)^{-\beta_g} e^{-\epsilon/T_g}, \quad (2)$$

with a temperature that decreases with distance beyond  $r_g$  like,  $T_g(r) \sim T(0) r_g^2 / (r_g^2 + r^2)$ , with,  $T(0) \sim 1$  eV, and  $\beta_g \sim 0$ . The observed energy of a glory photon which was scattered by an electron comoving with a CB at redshift  $z$ , is:

$$E = \frac{\gamma_0 \delta_0 \epsilon (1 + \cos \theta_{in})}{(1 + z)}, \quad (3)$$

where  $\theta_{in}$  is the angle of incidence of the initial photon onto the CB, in the SN rest system. For a quasi spherical distribution of scattered light,  $\cos \theta_{in}$  in Eq. (3) roughly averages to zero. The predicted time-dependent spectrum of the GRB pulse produced by ICS of the glory photons is given by (DD2004):

$$E \frac{dN_\gamma}{dE} \sim \left( \frac{E}{E_p(t)} \right)^{-\beta_g} e^{-E/E_p(t)} + b (1 - e^{-E/E_p(t)}) \left( \frac{E}{E_p(t)} \right)^{-p/2}, \quad (4)$$

where,

$$\begin{aligned} E_p(t) &\approx E_p(0) \frac{t_p^2}{(t^2 + t_p^2)}, \\ E_p(0) &\approx \frac{\gamma_0 \delta_0}{1 + z} T(0), \end{aligned} \quad (5)$$

with  $t_p \approx (1+z) r_g / c \gamma_0 \delta_0$ , being the peak time of  $dN_\gamma/dt$  discussed in the next chapter.

The first term in Eq. 4 with  $\beta_g \sim 0$ , is the result of Compton scattering by the bulk of the CB's electrons, which are comoving with it. The second term in Eq. (4) is induced by a very small fraction of 'knocked on' and Fermi accelerated electrons, whose initial spectrum (before Compton and synchrotron cooling) is  $dN_e/dE \propto E^{-p}$ , with  $p \approx 2.2$ . For  $b = \mathcal{O}(1)$ , the energy spectrum predicted by the CB model, Eq. (4), bears a striking resemblance to the Band function (Band et al. 1993) traditionally used to model the energy spectra of GRBs, but GRBs where the spectral measurements extended over a much wider energy range than that of BATSE and Swift/BAT, are better fit by Eq. 4 (e.g., Wigger et al. 2008).

---

<sup>2</sup> The CB arrives at the wind shortly after its emitted light, well before the scattered/reemitted CB light could have left the beaming cone ( $r/2c\gamma^2 \ll r/\gamma c$ ).

For many Swift GRBs the spectral observations do not extend to energies bigger than  $E_p(0)$ , or the value of  $b$  in Eq. (4) is relatively small, so that the first term of the equation provides a very good approximation. This term coincides with the ‘cut-off power-law’ spectrum which has also been recently used to model many GRB spectra. For  $b \sim 0$  and  $\beta_g \sim 0$  it yields a peak value of  $E^2 dN/dE$  at  $E_p(t)$  whose pulse averaged value is:

$$E_p \approx E_p(t_p) \approx 0.5 E_p(0) \approx 155 \frac{\gamma_0 \delta_0}{10^6} \frac{T(0)}{1 \text{ eV}} \frac{3.2}{1+z} \text{ keV}, \quad (6)$$

where the numerical result was obtained for the pulse shape discussed in the next subsection and the indicated typical values, including the mean redshift  $\langle z \rangle \approx 2.2$  of Swift’s long GRBs (Greiner: <http://www.mpe.mpg.de/~jcg/grbgen.html>). For  $b=1$  and  $\beta_g \sim 0$ ,  $E_p$  is larger by 50% than that given by Eq. (6). The predicted spectrum, as in Eq. (4), and range of  $E_p$  values as in Eq. (6), are in good agreement with the observations of BATSE, BeppoSAX, Konus-Wind, Integral, Suzaku and RHESSI which cover a much broader energy range than Swift<sup>3</sup>.

In the CB model XRFs are GRBs with similar values of  $\gamma_0$ , but viewed from angles  $\theta \gg 1/\gamma_0$  (DD2004, DDD2004a). This implies a smaller  $\delta_0$  in Eq. (1), and consequently the softer spectrum and relatively small  $E_p$  that define an XRF, see Eqs. (4,5). XRFs have light curves with wider and less rugged peaks than GRBs. This follows from the time dependence of the corresponding light-curves, which we discuss next.

### 3.2. The light curves of GRB and XRF pulses

After launch, as the CB propagates in the progenitor’s wind on its way to the ISM, its cross section increases, its density and the wind’s density decrease and consequently their opacities decrease. Let  $t$  be the time after launch of a CB as measured by a distant observer. Approximating the CB geometry by a cylindrical slab with the same radius, density and volume, and neglecting the spread in arrival times of ICS photons from the CB which entered it simultaneously, their arrival rate is given by:

$$\frac{dN_\gamma}{dt} = e^{-\tau_w} n_g(t) \sigma_T \pi R^2(t) \frac{[1 - e^{-\tau_{CB}}]}{\sigma_a}, \quad (7)$$

where  $\tau_w$  is the opacity of the wind at the CB location,  $\tau_{CB}$  is the effective opacity of the expanding CB encountered by a photon with energy  $E' = (1+z) E/\delta_0$  which begins crossing it

---

<sup>3</sup>Swift data can determine  $E_p$  only when it is well within its 15-350 detection range. This results in a biased sample of GRBs whose (measured)  $E_p$  is smaller than the average over the entire GRB population.

at a time  $t$ ,  $\sigma_a(E')$  is the photo-absorption cross section at energy  $E'$  and  $\sigma_T$  is the Thomson cross section. The density of the glory photons seen by a CB is quasi isotropic and decreases roughly like,  $n_g \propto 1/(r^2 + r_g^2)$ , where  $r_g$  is distance where the wind becomes transparent (optical thickness  $\sim 1$ ) to glory photons. At an early time,  $r \approx c \gamma_0 \delta_0 t / (1+z)$ . Consequently,  $n_g \propto 1/(t^2 + \Delta t^2)$ , where  $\Delta t = (1+z) r_g / c \gamma_0 \delta_0$ . Thus, the shape of an ICS pulse produced by a CB is given approximately by,

$$E \frac{d^2 N_\gamma}{dt dE} \propto e^{-\tau_w} n_g \pi R^2 [1 - e^{-R_{tr}^2/R^2}] E \frac{dN_\gamma}{dE}, \quad (8)$$

where  $R_{tr}$  is the radius of the CB at  $t = t_{tr}$ , when  $\tau_{CB} \approx 1$ . i.e., when it becomes transparent to the scattered radiation, and  $E dN_\gamma/dE$  is given by Eq. (4). The pre-supernova wind from the progenitor star produces a density distribution,  $n(r) = n_0 r_0^2 / r^2$  around it, which yields  $\tau_w = a(E)/t$  with  $a(E) = \sigma_a n_0 r_0^2 (1+z) / c \gamma_0 \delta_0$ . At sufficiently high energies the opacities of the wind and the CBs are mainly due to Compton scattering and then,  $R_{tr} \sim \sqrt{\sigma_T N_b / \pi}$ , where  $\sigma_T$  is the Thomson cross section and  $N_b$  is the baryon number of the expanding CB. At low energies, their opacity is dominated by free-free (ff) absorption because the CBs and the wind along their trajectory are completely ionized. In the CBs' rest frame the glory photons have typical energies,  $E' \ll \text{keV}$ . At such low energies, the opacity of CBs with a uniform density behaves like,  $\tau_{CB} \sim E'^{-3} (1 - e^{-E'/T'}) G(E') R^{-5}$ , where  $G(E')$  is the quantum mechanical Gaunt factor that depends logarithmically on  $E'$  (e.g., Lang 1980 and references therein). Thus, when the optical thickness of a CB is dominated by free-free photo-absorption, its transparency radius increases with decreasing energy like  $R_{tr} \propto E^{-3/5} = E^{-0.6}$  at  $E' \gg T'$  and  $R_{tr} \propto E^{-2/5} = E^{-0.4}$  at  $E' \ll T'$ , yielding  $R_{tr} \sim E^{-0.5 \pm 0.1}$ .

The initial rapid expansion of a CB slows down as it propagates through the wind and scatters its particles (DDD2002, DD2004). If this expansion is roughly described by,  $R^2 \approx R_{cb}^2 t^2 / (t^2 + t_{exp}^2)$ , where  $R_{cb}$  is the asymptotic radius of the CB and  $t_{exp} \gg t_{tr}$ , then, Eq. (8) can be approximated by,

$$E \frac{d^2 N_\gamma}{dt dE} \propto \frac{e^{-a/t} \Delta t^2 t^2}{(t^2 + \Delta t^2)(t^2 + t_{tr}^2)} E \frac{dN_\gamma}{dE}. \quad (9)$$

For nearly transparent winds ( $a \rightarrow 0$ ) and for  $t_{tr} \sim \Delta t$ , Eq. (9) has an approximate shape,

$$E \frac{d^2 N_\gamma}{dt dE} \propto \frac{\Delta t^2 t^2}{(t^2 + \Delta t^2)^2} E \frac{dN_\gamma}{dE}, \quad (10)$$

which peaks around  $t \approx \Delta t$ . Except for very early times, this shape is almost undistinguishable from that of the ‘Master’ formula of the CB model (DD2004),

$$E \frac{d^2 N_\gamma}{dt dE} \propto e^{-\Delta t^2/t^2} [1 - e^{-\Delta t^2/t^2}] E \frac{dN_\gamma}{dE}, \quad (11)$$

which took into account also arrival time effects that depend on the geometry of the CB and the observer’s viewing angle, and was shown to well describe the prompt emission pulses of LGRBs (DD2004) and the rapid decay with a fast spectral softening of their prompt emission (DDD2008a).

At the relatively low X-ray energies covered by Swift and, more so, at smaller ones, the first term on the RHS of Eq. (4) usually dominates  $E dN_\gamma/dE$ . Consequently, the light curve generated by a sum of ICS pulses at a luminosity distance  $D_L$  is generally well approximated by:

$$E \frac{d^2 N_\gamma}{dt dE} \approx \sum_i A_i \Theta[t-t_i] \frac{\Delta t_i^2 (t-t_i)^2}{((t-t_i)^2 + \Delta t_i^2)^2} e^{-E/E_{p,i}[t-t_i]}, \quad (12)$$

where the index ‘i’ denotes the i-th pulse produced by a CB launched at an observer time  $t=t_i$ , or, alternatively,

$$E \frac{d^2 N_\gamma}{dt dE} \approx \sum_i A_i \Theta[t-t_i] e^{-\Delta t_i^2/(t-t_i)^2} [1 - e^{-\Delta t_i^2/(t-t_i)^2}] e^{-E/E_{p,i}[t-t_i]}, \quad (13)$$

where  $E_{p,i}[t-t_i]$  is given by Eq. (5) with  $t$  replaced by  $t-t_i$  and,

$$A_i \approx \frac{c n_g(0) \pi R_{CB}^2 \gamma_0 \delta_0^3 (1+z)}{4 \pi D_L^2}. \quad (14)$$

Thus, in the CB model, each ICS pulse in the GRB light curve is effectively described by four parameters,  $t_i$ ,  $A_i$ ,  $\Delta t_i$  and  $E_{p,i}(0)$ , which are best fit to reproduce its observed light curve.

Setting  $t_i = 0$ ,  $E_p(t)$  has the approximate form  $E_p(t) \approx E_p t_p^2/t^2$ . Such an evolution has been observed in the time resolved spectrum of well isolated pulses (see, for instance, the insert in Fig. 8 of Mangano et al. 2007), until the ICS emission is overtaken by the broad band synchrotron emission from the swept-in ISM electrons. Hence, the temporal behaviour of the separate ICS peaks is given by:

$$E \frac{d^2 N_\gamma}{dt dE}(E, t) \propto \frac{t^2/\Delta t^2}{(1 + t^2/\Delta t^2)^2} e^{-E t^2/E_p t_p^2} \approx F(E t^2), \quad (15)$$

to which we shall refer as the ‘ $E t^2$  law’. A simple consequence of this law is that unabsorbed ICS peaks have approximately identical shape at different energies when plotted as function of  $E t^2$ .

A few other trivial but important consequences of Eq. (15) for unabsorbed GRB peaks at  $E \lesssim E_p$  are the following:

- The peak time of a pulse is at,

$$t_p = t_i + \Delta t_i. \quad (16)$$

- The full width at half maximum (FWHM) of a pulse is,

$$\text{FWHM} \approx 2 \Delta t_i, \quad (17)$$

and it extends from  $t \approx t_i + 0.41 \Delta t_i$  to  $t \approx t_i + 2.41 \Delta t_i$ .

- The rise time (RT) from half peak value to peak value satisfies,

$$\text{RT} \approx 0.30 \text{ FWHM}, \quad (18)$$

independent of energy. It agrees with the empirical relation that was inferred by Kocevski et al. (2003) from BATSE bright GRBs,  $\text{RT} \approx (0.32 \pm 0.06) \text{ FWHM}$ .

- The FWHM increases with decreasing energy approximately like a power-law,

$$\text{FWHM}(E) \sim E^{-0.5}. \quad (19)$$

This relation is consistent with the empirical relation,  $\text{FWHM}(E) \propto E^{-0.42 \pm 0.06}$ , satisfied by BATSE GRBs (Fenimore et al. 2003).

- The onset-time,  $t_i$ , of a pulse is simultaneous at all energies. But the peak times  $t_p$  at different energies differ and the lower-energy ones ‘lag’ behind the higher-energy ones:

$$t_p - t_i \propto E^{-0.5}. \quad (20)$$

- The time averaged value of  $E_p(t)$  for GRB peaks, which follows from Eq. (5), satisfies:

$$E_p = E_p(0)/2 = E_p(t_p). \quad (21)$$

### 3.3. X-ray ‘flares’ and $\gamma$ -ray pulses

In more than 50% of the GRBs observed by Swift, the X-ray light curve, during the prompt GRB and its early AG phase, shows flares superimposed on a smooth background. In the CB model, an X-ray ‘flare’ coincident in time with a  $\gamma$ -ray pulse is simply its low-energy tail. They are both due to Compton scattering of photons in the thin-bremsstrahlung glory. The glory’s photons incident on the CB at small  $\epsilon_i$  or  $1 + \cos \theta_i$  result in X-ray or softer up-scattered energies, see Eq. (3). The harder and less collinear photons result in  $\gamma$ -rays. The light-curve and spectral evolution of an ICS X-ray flare are given approximately by Eq. (12). Its width is related to that of the accompanying  $\gamma$ -ray pulse as in Eq. (17). Relative to its  $\gamma$ -ray counterpart, an X-ray flare is wider and its peak time ‘lags’, after the peak time of the

gamma-ray pulse. The X-ray flares during a GRB are well separated only if the  $\gamma$ -pulses are sufficiently spaced.

In the CB model, X-ray flares without an accompanying detectable  $\gamma$ -ray emission can be of two kinds. They can be ICS flares produced by CBs ejected with relatively small Lorentz factors and/or relatively large viewing angles (Dado et al. 2004). Such CBs may be ejected in accretion episodes both during the prompt GRB and in delayed accretion episodes onto the newly formed central object in core collapse SNe (De Rújula 1987). ICS flares satisfy the  $E t^2$ -law and exhibit a rapid softening during their fast decline phase which is well described by Eqs. (4,5), as shown in detail in DDD2008b.

We shall see in our case studies that very often, during the rapidly decreasing phase of the prompt emission, there are ‘mini X-ray flares’ which show this rapid spectral softening. As the accretion material is consumed, one may expect the ‘engine’ to have a few progressively-weakening dying pangs.

Flares can also be due to enhanced synchrotron emission during the passage of CBs through over-densities produced by mass ejections from the progenitor star or by interstellar winds (DDD2002a, DDD2003a). Synchrotron emission from CBs are discussed in the following section. Late flares seem to have the predicted synchrotron spectrum and spectral evolution which are different from those of ICS flares.

#### 4. Synchrotron radiation

A second mechanism besides ICS, which generates radiation from a CB, is synchrotron radiation (SR). A CB encounters matter in its voyage through the interstellar medium (ISM), effectively ionized by the high-energy radiation of the very same CB. This continuous collision with the medium decelerates the CB in a characteristic fashion, and results in a gradual steepening of the light curves of their emitted synchrotron radiation (DDD2002a). In §4.1, we review the calculation of  $\gamma(t)$ , the CB’s diminishing Lorentz factor. We have assumed and tested observationally, via its CB-model consequences, that the impinging ISM generates within the CB a turbulent magnetic field<sup>4</sup>, in approximate energy equipartition with the energy of the intercepted ISM (DDD2002a, DDD2003a). In this field, the intercepted electrons emit synchrotron radiation. This radiation, isotropic in the CB’s rest frame, is

---

<sup>4</sup>‘First principle’ numerical simulations of two plasmas merging at a relative relativistic Lorentz factor (Frederiksen et al. 2003, 2004, Nishikawa et al. 2003) do not generate the desired shocks, but do generate turbulently moving magnetic fields.

Doppler boosted and collimated around the direction of motion into a cone of characteristic opening angle  $\theta(t) \sim 1/\gamma(t)$ . In §4.2 we summarize the predictions of the synchrotron radiation’s dependence on time and frequency (DDD2002a, DDD2003a).

#### 4.1. The deceleration of a CB

As it ploughs through the ionized ISM, a CB gathers and scatters its constituent ions, mainly protons. These encounters are ‘collisionless’ since, at about the time it becomes transparent to radiation, a CB also becomes ‘transparent’ to hadronic interactions (DD2004). The scattered and re-emitted protons exert an inward pressure on the CB, countering its expansion. In the approximation of isotropic re-emission in the CB’s rest frame and a constant ISM density  $n \sim n_e \sim n_p$ , one finds that within minutes of observer’s time  $t$ , a typical CB of baryon number  $N_b \approx 10^{50}$  reaches an approximately constant ‘coasting’ asymptotic radius  $R \sim 10^{14}$  cm, before it finally stops and blows up, after a journey of years of observer’s time. During the coasting phase, and in a constant density ISM,  $\gamma(t)$  obeys (DDD2002a, Dado et al. 2006):

$$(\gamma_0/\gamma)^{3+\kappa} + (3 - \kappa) \theta^2 \gamma_0^2 (\gamma_0/\gamma)^{1+\kappa} = 1 + (3 - \kappa) \theta^2 \gamma_0^2 t/t_0, \quad (22)$$

with

$$t_0 = \frac{(1+z) N_B}{(6+2\kappa) c n \pi R^2 \gamma_0^3}, \quad (23)$$

where the numerical value  $\kappa=1$ , is for the case in which the ISM particles re-emitted fast by the CB are a small fraction of the flux of the intercepted ones and  $\kappa=0$  in the opposite limit. In the CB model of cosmic rays (Dar & De Rújula 2006) the observed spectrum strongly favours  $\kappa=1$ . Thus in all of our fits we use  $\kappa=1$ , though the results are not decisively sensitive to this choice. As can be seen from Eq. (22),  $\gamma$  and  $\delta$  change little as long as  $t < t_b = [1 + 2\gamma_0^2 \theta^2] t_0$ . where, in terms of typical CB-model values of  $\gamma_0$ ,  $R$ ,  $N_B$  and  $n$ ,

$$t_b = (1300 \text{ s}) [1 + 2\gamma_0^2 \theta^2] (1+z) \left[ \frac{\gamma_0}{10^3} \right]^{-3} \left[ \frac{n}{10^{-2} \text{ cm}^{-3}} \right]^{-1} \left[ \frac{R}{10^{14} \text{ cm}} \right]^{-2} \left[ \frac{N_B}{10^{50}} \right]. \quad (24)$$

For  $t \gg t_b$ ,  $\gamma$  and  $\delta$  decrease like  $t^{-1/4}$ .

The deceleration equation for a non-expanding CB can be integrated analytically also for other commonly encountered density profiles, such as a step function  $n(r) \propto 1/r^2$ . Such a profile is produced by a constant blowing wind from a massive progenitor star prior to the GRB, or from a star formation region, or in an isothermal sphere which describes quite well the density distribution in galactic bulges, galactic halos and elliptical galaxies. Due to lack of space they will not be discussed here. In the general case, the deceleration equation can be integrated numerically.

## 4.2. The Synchrotron spectral energy density

As indicated by first-principle calculations of the relativistic merger of two plasmas (Frederiksen et al. 2004), the ISM ions continuously impinging on a CB generate within it turbulent magnetic fields, which we assume to be in approximate energy equipartition with their energy,  $B \approx \sqrt{4\pi n m_p c^2} \gamma$ . In this field, the intercepted electrons emit synchrotron radiation. The SR, isotropic in the CB's rest frame, has a characteristic frequency,  $\nu_b(t)$ , the typical frequency radiated by the electrons that enter a CB at time  $t$  with a relative Lorentz factor  $\gamma(t)$ . In the observer's frame:

$$\nu_b(t) \simeq \frac{\nu_0}{1+z} \frac{[\gamma(t)]^3 \delta(t)}{10^{12}} \left[ \frac{n}{10^{-2} \text{ cm}^3} \right]^{1/2} \text{ Hz.} \quad (25)$$

where  $\nu_0 \simeq 3.85 \times 10^{16} \text{ Hz} \simeq 160 \text{ eV}$ . The spectral energy density of the SR from a single CB at a luminosity distance  $D_L$  is given by (DDD2003a):

$$F_\nu \simeq \frac{\eta \pi R^2 n m_e c^3 \gamma(t)^2 \delta(t)^4 A(\nu, t)}{4 \pi D_L^2 \nu_b(t)} \frac{p-2}{p-1} \left[ \frac{\nu}{\nu_b(t)} \right]^{-1/2} \left[ 1 + \frac{\nu}{\nu_b(t)} \right]^{-(p-1)/2}, \quad (26)$$

where  $p \sim 2.2$  is the typical spectral index<sup>5</sup> of the Fermi accelerated electrons,  $\eta \approx 1$  is the fraction of the impinging ISM electron energy that is synchrotron re-radiated by the CB, and  $A(\nu, t)$  is the attenuation of photons of observed frequency  $\nu$  along the line of sight through the CB, the host galaxy (HG), the intergalactic medium (IGM) and the Milky Way (MW):

$$A(\nu, t) = \exp[-\tau_\nu(\text{CB}) - \tau_\nu(\text{HG}) - \tau_\nu(\text{IGM}) - \tau_\nu(\text{MW})]. \quad (27)$$

The opacity  $\tau_\nu(\text{CB})$  at very early times, during the fast-expansion phase of the CB, may strongly depend on time and frequency. The opacity of the circumburst medium [ $\tau_\nu(\text{HG})$  at early times] is affected by the GRB and could also be  $t$ - and  $\nu$ -dependent. The opacities  $\tau_\nu(\text{HG})$  and  $\tau_\nu(\text{IGM})$  should be functions of  $t$  and  $\nu$ , for the line of sight to the CBs varies during the AG observations, due to the hyperluminal motion of CBs.

The dependence of the SR afterglow, on the CB's radius, external density and external extinction, as summarized in Eq. (26), give rise to a variety of early time optical light curves, in contrast to the more uniform behaviour of the optical and X-ray SR afterglow at later times.

---

<sup>5</sup>The normalization in Eq. (25) is only correct for  $p > 2$ , for otherwise the norm diverges. The cutoffs for the  $\nu$  distribution are time-dependent, dictated by the acceleration and SR cooling times of electrons and their 'Larmor' limit. The discussion of these processes being complex (DD2003a, DD2006), we shall satisfy ourselves here with the statement that for  $p \leq 2$  the AG's normalization is not predicted.

### 4.3. The X-ray afterglow

The Swift X-ray band is usually above the bend frequency  $\nu_b$ , as given by Eq. (25), at all times. It then follows from Eq. (26) that the spectral energy density of the *unabsorbed* X-ray afterglow has the form:

$$F_\nu \propto R^2 n^{(p+2)/4} \gamma^{(3p-2)/2} \delta^{(p+6)/2} \nu^{-p/2} = R^2 n^{\Gamma/2} \gamma^{3\Gamma-4} \delta^{\Gamma+2} \nu^{-\Gamma+1}, \quad (28)$$

where we have used the customary notation  $dN_\gamma/dE \sim E^{-\Gamma}$ . For a constant density, the deceleration of the CB, which causes transition of  $\gamma$  and  $\delta$  around  $t = t_b$  from a constant value to an asymptotic power law decline,  $\delta \propto \gamma \propto t^{-1/4}$  at  $t \gg t_b$ , induces a bend/gradual break in the synchrotron AG of a CB around  $t = t_b$  from a plateau to an asymptotic power-law decay,

$$F_\nu \propto t^{-p/2-1/2} \nu^{-p/2} = t^{-\Gamma+1/2} \nu^{-\Gamma+1}, \quad (29)$$

with a power-law in time steeper by half a unit than that in frequency. In terms of the frequently used notation, the asymptotic behaviour  $F_\nu(t) \propto t^{-\alpha} \nu^{-\beta}$ , satisfies,

$$\alpha = \beta + 1/2 = p/2 + 1/2 = \Gamma - 1/2. \quad (30)$$

which is valid only for a constant density.

For a fast falling density beyond a distance  $r_c$ , seen by CBs which encounter density bumps due to stellar winds or by CBs which escape the galactic bulge or disk into the galactic halo,  $\gamma$  and  $\delta$  tend to a constant and  $r - r_c$  becomes proportional to  $t - t_c$  where  $r(t_c) = r_c$ . As a result, for a density profile  $n \propto 1/r^2$  beyond  $r_c$  the unattenuated synchrotron afterglow, as given by Eq. (28), tends to,

$$F_\nu \propto n^{(p+2)/4} \nu^{-p/2} \propto (t - t_c)^{-(p+2)/2} \nu^{-p/2} = (t - t_c)^{-\Gamma} \nu^{-\Gamma+1}, \quad (31)$$

and satisfies the asymptotic relation,

$$\alpha = \beta + 1 = \Gamma \approx 2.1. \quad (32)$$

Thus, unattenuated optical and X-ray AGs of GRBs, may steepen at late times to an asymptotic  $\sim (t - t_c)^{-2.1}$  decline. Such an achromatic steepening, which was seen in several late time optical and X-ray AGs of Swift GRBs (see Figs. 6,7), may have been misinterpreted as very late ‘jet breaks’ (e.g., Dai et al. 2008, Racusin et al. 2008a).

All the late time afterglows of Swift GRBs which are well sampled at late time seem to satisfy well (see DDD2008b) either the asymptotic relation (30) or (32).

#### 4.4. Early-time SR

During its early-time emission, when both  $\gamma$  and  $\delta$  stay put at their initial values  $\gamma_0$  and  $\delta_0$ , Eq. (26) yields an early-time SR light curve,  $F_\nu \propto e^{-\tau_w} R^2 n^{(1+\beta)/2} \nu^{-\beta}$ . Since  $r \propto t$ , a CB ejected into a windy density profile,  $n \propto 1/r^2$ , created by the mass ejection from the progenitor star prior to its SN explosion, emit SR with an early-time light curve,

$$F_\nu \propto \frac{e^{-a/t} t^{1-\beta}}{t^2 + t_{exp}^2} \nu^{-\beta}. \quad (33)$$

For a CB ejected at time  $t_i$ , the time  $t$  must be replaced by,  $t - t_i$ , the time after ejection.

In the  $\gamma$ -ray and X-ray bands, the SR emission from a CB is usually hidden under the prompt ICS emission. But in many GRBs the asymptotic exponential decline of the energy flux density of the prompt ICS emission,  $F_\nu \propto t^{-2} e^{-Et^2/E_p t_p^2}$ , is taken over by the slower power-law decline,  $F_\nu \propto t^{-\Gamma}$ , of the synchrotron emission in the windy  $\sim 1/r^2$  circumburst density before the CB reaches the constant ISM density and the AG emission enters the plateau phase. This is demonstrated in Fig. 3 for GRBs 051021B, 060211A, 061110A, 070220, 080303, 080307. As soon as the light curve is dominated by SR, the rapid spectral softening of the ICS dominated light curve stops and the spectrum of the unabsorbed X-ray emission changes to the ordinary synchrotron power-law spectrum with the typical power-law index,  $\beta_X \approx 1.1$  ( $\Gamma \approx 2.1$ ). Unlike the sudden change in the spectrum when the prompt ICS emission is taken over by SR only in the plateau phase, there is no spectral change when SR dominates the X-ray light curve already before the plateau phase.

When the windy density changes to a constant ISM density, the light curve of the early-time optical AG as given by Eq. (33) changes to a plateau/shallow decline with a typical SR optical spectrum. After the deceleration bend/break, the temporal decline of the optical afterglow begins to approach that of the X-ray AG because the bend frequency, which decreases like  $\nu_b \propto \sqrt{n} \gamma^3 \delta$ , crosses below the optical band. After the cross-over,  $\beta_O(t) \approx \beta_X \approx 1.1$  and the AG becomes achromatic and approaches the asymptotic power-law decay,  $F_\nu \sim t^{-\beta_X - 1/2}$ , yielding an optical AG with a similar early time and late-time power-law decay,  $F_\nu \sim t^{-1.6}$ . This behaviour has been observed in several very bright GRBs whose optical light curve was discovered early enough and was followed until late time, e.g., in GRBs 990123, 021212, 061007, 061126 and 080319B (see Fig. 2).

Unlike the prompt  $\gamma$ -ray and X-ray emission in ordinary GRBs, which is dominated by ICS, their prompt optical emission is usually dominated by SR. This is because  $F_\nu$  of SR increases with decreasing frequency like  $\nu^{-\beta_O}$  with  $\beta_O \sim 0.5$ , whereas the prompt ICS emission for  $h\nu \ll E_p$  is independent of frequency ( $\beta \approx 0$ ). The entire diversity of the chromatic early-time optical light curves of LGRBs which were measured with robotic telescopes, such

as GRBs 030418 (Rykoff et al. 2004), 050319 (Wozniak et al. 2005, Quimby et al. 2006a), 050820A (Cenko et al. 2006, Vestrand et al. 2006), 060418 (Molinari et al. 2007) 060605 (Ferrero et al. 2008), 060607A (Molinari et al. 2007, Nysewander et al. 2007, Ziaepour et al. 2008) 0701010A (Covino et al. 2008), and 061126 (Perley et al. 2008; Gomboc et al. 2008), is described well by Eq. (33). This is demonstrated in Figs. 5,8.

$F_\nu$  for SR is proportional to  $\delta^{3+\beta}$ . Unlike GRBs with  $\delta_0 \sim \gamma_0$ , XRFs have  $\delta_0 \ll \gamma_0$ , and consequently their prompt optical emission is also dominated by ICS. An optical pulse dominated by ICS emission, is distinguishable from a pulse dominated by SR by pulse shape, spectrum and spectral evolution. The optical ICS peaks satisfy the approximate ‘ $E \times t^2$  law’, they are much wider than their  $\gamma$ -ray and X-ray counterparts and as a result they are usually blended. However, in XRFs such as 060218 and 080109, the ICS optical peak has a large lagtime and is clearly visible as humps in the light curves at different optical wave-lengths (see Fig. 9).

#### 4.5. Chromatic Afterglows

The early-time light curves of LGRBs are very chromatic because their prompt  $\gamma$ -ray and X-ray emission is dominated ICS pulses while their optical emission is dominated by SR with entirely different temporal and spectral properties. The light curves of ICS that satisfy the ‘ $E t^2$  law’ are by themselves very chromatic and, yield very chromatic afterglows even for XRFs where the prompt optical emission is also dominated by ICS (see Figs. 9,??).

In the CB model, SR dominates the afterglow emission at all wavelengths both in GRBs and XRFs. The observed chromatic behaviour of the afterglow results from its dependence on the circumburst density, the bend frequency and light attenuation along the line of sight to the source of the AG. The general behaviour which takes into account light attenuation inside the CBs and in the circumburst environment, CB expansion and density variation, as summarized in Eq. (26), and the chromatic light curves of superimposed flares, is complex and will not be discussed in detail in this paper. The behaviour becomes simpler when the CB and circumburst medium become transparent to radiation and the fast expansion of the CB has slowed down.

For a constant circumburst density, the simplest situation arises when all observed frequencies are above the injection bend; Notice that for typical reference parameters,  $\nu_b(0)$  in Eq. (25) corresponds to an energy well above the UVO bands. But there are cases where  $\delta$  is sufficiently small (e.g., in XRFs and GRBs with very small  $E_{iso}^\gamma$ ) and/or  $n$  is very small, such that  $\nu_b(0) \propto \sqrt{n} \gamma_0^3 \delta_0$ , is already below the UVO bands. In that case the (unattenuated)

synchrotron spectrum stays put at  $F_\nu \sim \nu^{-p/2}$ , see Eq. (26), and is achromatic all the way from the UVO bands to X-rays at all times.

In ordinary GRBs,  $\nu_b(0)$  in Eq. (25) is usually well above the UVO bands, but below the X-ray band. In that case, the unabsorbed spectrum of the optical AG evolves in a predicted fashion from  $F_\nu \propto [\nu/\nu_b(t)]^{-1/2}$  to  $F_\nu \propto [\nu/\nu_b(t)]^{-p/2}$  that of the unabsorbed X-ray AG. Many cases of this very specific chromatic evolution have been studied in DDD2003a. The success of their CB-model description corroborates the assumption that the CB's inner magnetic-field intensity  $B(t)$ , of which  $\nu_b(t)$  is a function, is approximately determined by the equipartition hypothesis.

In a constant density, the CBs begin to decelerate rapidly around  $t_b$  of Eq. (24). Consequently, the bend frequency,  $\nu_b(t) \propto \gamma^3 \delta$ , declines rapidly with time beyond  $t_b$  and crosses below the optical band. According to Eqs. (24,26),  $F_\nu$  steepens around  $t_b$  to an asymptotic achromatic power-law decline,  $F_\nu \propto \nu^{-\beta} t^{-\alpha}$  with  $\alpha \approx \beta+1/2 = \Gamma-1/2$ , all the way from X-rays to the UVO bands, This smooth CB-deceleration bend/break in the AG of canonical GRBs beyond which the XUVO AG becomes achromatic is not to be confused with the achromatic *break* predicted in fireball models (Rhoads 1997, 1999). The CB model interpretation of this well understood achromatic bend-time (see, e.g., DDD2003a) is further strengthened by the facts that it is observed at the predicted time scale and displays the predicted correlations with the prompt GRB emission (DDD 2008b), and that the predicted asymptotic relations between the temporal and spectral power-law declines beyond it are well satisfied.

A variation of the chromatic behaviour due to bend-frequency crossing occurs when it happens early enough for the circumburst density profile to be still dominated by the progenitor's pre-SN wind emissions. At early times,  $t \ll t_b$ , the deceleration of CBs has not significantly affected their motion and  $\gamma(t)$  and  $\delta(t)$  are practically constant. Yet, the observer's bend frequency,  $\nu_b(t) \propto \sqrt{n(t)} [\gamma(t)]^3 \delta(t)$ , decreases with time as  $n(t)$  varies. Keeping track of the  $n$ -dependence, we concluded (DDD2003a) from Eqs. (25,26) that the unattenuated early synchrotron radiation of a CB moving in a windy density profile,  $n \sim r^{-2} \sim t^{-2}$ , is given approximately by:

$$F_\nu \propto n^{(1+\beta)/2} \nu^{-\beta} \propto t^{-(1+\beta)} \nu^{-\beta}. \quad (34)$$

In cases for which  $\nu_b(0)$  is initially well above the UVOIR bands,  $\beta \approx 0.5$ , and the initial UVOIR behaviour is  $F_\nu \propto t^{-1.5} \nu^{-0.5}$ , while the X-ray AG, for which  $\nu_b \ll \nu$  and  $\beta \simeq 1.1$ , behaves like  $F_\nu \propto t^{-2.1} \nu^{-1.1}$  (DDD2003b). If the density continues to decline like  $1/r^2$ , then the bend frequency crosses below the UVOIR band, and the XUVOIR AG becomes achromatic with  $\alpha \approx \beta+1 = \Gamma \sim 2.1$ .

Optical light curves with the expected power-law decay,  $F_\nu \sim t^{-1.5}$ , after an initial fast rise, have been observed, e.g., in GRB 990123 (Akerlof et al. 1999); GRB 021211 (Li et

al. 2003) and GRB 061126 (Perley et al. 2008). Usually, the steeper  $F_\nu \sim t^{-(1+\beta_x)} \sim t^{-2.1}$  early time decline of the X-ray synchrotron emission is hidden under the dominant early-time ICS emission, but, in several GRBs it is visible as a power-law tail that takes over the initial exponential decay of the ICS pulse (see Fig. 3). This take-over also stops the fast spectral softening of the ICS dominated light curve and changes the soft spectrum into the typical harder SR spectrum.

In the CB model, the extinction in the host galaxy, which is frequency dependent, can also be time dependent even far from the burst environment. In a day of the highly aberrated observer’s time, CBs typically move to a few hundred parsec distances from their birthplace, a region wherein the frequency dependent extinction should have drastically diminished. A strong variation in extinction at early times was observed, e.g., by Perley et al. (2008) in GRB 061126, by Molinari et al. (2007) and Nysewander et al. (2007) in GRB 06060A and by Ferrero et al. (2008) in GRB 060605. The frequency dependence of the extinction which changes with the changing line of sight to the moving CB in the host galaxy, can change an original achromatic AG into an observed chromatic AG.

Finally, the ICS, which dominates also the prompt optical emission in XRFs with  $\delta_0 \ll \gamma_0$ , results in a very specific chromatic behaviour: the X-ray light curve is declining rapidly, while the optical light curves are stretched by the  $E t^2$  law and display humps that are nothing but the X-ray pulse(s) whose peak time and width are stretched by the  $E \times t^2$  ‘law’. A striking example of this very chromatic behaviour is shown in Fig. (9) for XRF 060218, discussed in more detail in §5.1.

Because of the complex chromatic behaviour of GRB afterglows, we have limited our discussion to the chromatic properties of the AG of a single CB. The actual situation can be much more complex because the afterglow, like the prompt emission, is usually the sum of the contributions from many individual CBs ejected at slightly different times with different parameters (baryon number, Lorentz factor and emission angle) which have or have not merged by the time of the afterglow phase. For the sake of simplicity, brevity and predictivity, we shall assume that the AG from the entire ensemble of CBs can be calculated as if it was due to a single one or two effective CBs during the AG phase. Despite this simplification, the CB model, as we shall show, can well explain and reproduce, within observational uncertainties, the entire diversity of the measured light curves of the Swift GRBs and their afterglows.

## 5. Comparison with Observations

To date, Swift has detected over 350 long GRBs, localized them through their  $\gamma$ , X-ray and UVO emissions and followed most of them until they faded into the background. Beside the Swift observations, there have been many prompt optical measurements of Swift GRBs by an increasing number of ground-based robotic telescopes, and follow-up measurements by other ground-based optical telescopes, including some of the largest ones. Incapable of discussing all Swift GRBs, we discuss only a sample of 33 GRBs ( $\approx 10\%$  of all Swift GRBs), which have a well sampled X-ray and optical light curves from early to late time and which well represent the entire diversity of Swift GRBs.

We fit the X-ray light curves as reported in the Swift/XRT GRB light curve repository ([http://www.swift.ac.uk/xrt\\_curves/](http://www.swift.ac.uk/xrt_curves/); Evans et al. 2007). We used Eq. (12) or Eq. (13) for the early time ICS contribution, and Eq. (26) for the SR afterglow with its simple explicit limit, Eq. (33), for the very early time synchrotron emission. The a-priori unknown parameters are the number of CBs, their ejection time, baryon number, Lorentz factor and viewing angle and the environmental ones along the CBs' trajectory, i.e. the distributions of the glory's light and of the ISM density. To demonstrate that the CB model correctly describes all of the observed features of the Swift X-ray observations, it suffices to include in the fits only the main or the latest few observed pulses or flares in the prompt emission. This is because the exponential factor in Eq. (12) suppresses very fast the relative contribution of the earlier pulses by the time the data sample the later pulses or flares. It also suffices to fix the glory's light and ISM density distribution to be the same along the trajectories of all CBs in a given GRB. The pulse shapes are assumed to be universal: given by Eq. (12). For the synchrotron contribution, in most cases it suffices to consider a common emission angle  $\theta$  and an average initial Lorentz factor  $\gamma_0$  for the ensemble of CBs.

The ISM density along the CBs' trajectories was generally taken to have a windy' contribution ( $\propto 1/r^2$ ) near the ejection site which is taken over later by a constant ISM density. The windy density is only relevant in some optical synchrotron-dominated AGs for which very early data are available, as discussed in the previous section. Density bumps with a density decline,  $n \propto 1/r^2$ , were assumed to generate X-ray and optical flares in the synchrotron emission at late times (DDD2003). Only for a small number ( $\sim 14$  out of 350 Swift GRBs) the observed late time decline could not be well fit unless a transition from a constant density to a density proportional to  $1/r^2$  was assumed.

The X-ray and optical light-curves were calculated with the same CB parameters. The spectral index  $p$  of the Fermi-accelerated electrons in the CBs, was treated as a free parameter. In the CB model, it determines both the spectral and temporal declines of the AG, as in Eq. (26). In cases where the fit was insensitive to  $p$  we fixed its value to be the canonical

value (DDD2002)  $p=2.2$ . The relative normalization of the X-ray and optical afterglows was generally treated as a free adjustable parameter except when both extinction of the optical light and absorption of the emitted X-rays could be estimated reliably. In such cases the predicted dependence on frequency could be tested. Such cases include prompt ICS flares and the late-time SR afterglow where both the X-ray band and the optical band are above the bend frequency and the SR afterglow becomes ‘achromatic’. No attempt was made to derive the environmental parameters, because the use of simplifying assumptions, the single CB approximation and the lack of exact knowledge of the extinction of the optical radiation in the host galaxy, make such attempts unreliable.

In the following case studies of a representative sample of the entire diversity of Swift GRBs, we include GRBs with canonical, non-canonical and semi-canonical light curves, with or without superimposed flares, GRBs with very chromatic early time ‘afterglows, GRBs with exceptional rapidly decaying late afterglows and GRBs with very complex and chromatic light curves. Special attention is given to XRF 060218. The parameters used in the CB model description of the ICS flares and the synchrotron afterglow of all the above GRBs and XRFs to be discussed anon are listed in Tables 1 and 2.

## 5.1. Case Studies

### 5.1.1. GRBs with a canonical X-ray light curve

**GRB 060729.** *X-ray observations:* This GRB with a canonical X-ray light curve is described and discussed in detail in Grupe et al. 2007. It was detected and located by Swift at UT 19:12:29 July 29, 2006 (Grupe et al. 2006). It is one of the brightest Swift GRB in X-rays and has the longest follow-up observations in X-rays: more than 125 days after burst. The X-ray observations were triggered by the detection of a GRB precursor by the BAT, which dropped into the background level within 6 s. Two other major overlapping peaks were detected 70 s after trigger and a fourth one around 120 s. The end of the fourth peak was seen also by the XRT at the beginning of its observations. The XRT detected another flare around 180 s after which the light curve decayed rapidly by three orders of magnitude before it was overtaken by the plateau at  $530 \pm 25$  s, which lasted for  $\sim 1/2$  day before it bent into a power-law decline. During the fast decline of the prompt emission, the X-ray spectrum changed dramatically from a hard spectrum to a very soft one. After this phase the unabsorbed spectrum of the X-ray afterglow hardened to a power-law with  $\beta_X = 1.1$  and remained unchanged during the plateau phase and the late power-law decline. The complete light-curve obtained from the observations with the BAT (extrapolated to the XRT band), the XRT and XMM-Newton is shown in Fig. 1a; a magnified view of the early times light

curve is shown in Fig. 1b.

**GRB 060729.** *Interpretation:* The CB model fit to the complete X-ray light curve of GRB 060729 is shown in Fig. 1a. The overall good agreement between theory and observations extends over some eight orders of magnitudes in time and in flux. The spectral evolution of the X-ray emission is also in good agreement with the CB-model predictions (see DDD2008b). In the XRT 0.3-10 keV band the spectrum of the early time flares and their spectral evolution are well described by the exponential cut-off power-law obtained by ICS of a thin thermal bremsstrahlung spectrum, Eq. (12). In particular the exponential factor in Eq. (12) describes well the rapid softening of the spectrum as a function of time during the fast decaying phase of the burst (see DDD2008b). But, as soon as the X-ray afterglow is taken over by the synchrotron emission around 325 s its unabsorbed spectrum changes to the much harder SR power-law spectrum with  $\beta_X = 1.1$ . The temporal shape of the AG is best fit with electron spectral index  $p = 2.20$ , which implies  $\beta_X = 1.1$ , in good agreement with the observations of the XRT and of XMM-Newton (Grupe et al. 2007). The late power law decay satisfies the CB model prediction,  $\alpha = \Gamma - 1/2$ .

**GRB 060729.** *Optical observations and a sketch of their interpretation:* The ROTSE-IIIa telescope in Australia took a first 5 s image of this GRB, starting about a minute after the burst, which showed no afterglow down to magnitude 16.6. Some 23 s later, an AG of magnitude 15.7 was clearly detected. The AG brightened over several minutes, and faded very slowly (Quimby et al. 2006b). In the CB model such a behaviour is expected from the early synchrotron emission (Eq. (33)) in the UVOIR band during and shortly after the prompt GRB. The UVOT followed the UVO emission from 739 s after trigger until 20 days after burst. The VLT in Chile obtained spectra, and determined a relatively low redshift of  $z = 0.54$  for this burst (Theone et al. 2006). The light curves of its UVO AG show a striking similarity to the X-ray light curve (Grupe et al. 2007) as predicted by the CB model for the optical AG when the bending frequency is below the UVO band, and the extinction along the lines of sight to the hyperluminal CBs stays constant. All in all, the well sampled observations of the XUVO light curves of GRB 060729 agree well with the expectations of the CB model.

**GRB 061121.** *Observations* This canonical GRB at  $z = 1.314$  was described and discussed in detail in Page et al. 2007. It is one of the brightest GRBs in X-rays observed to date by the XRT. The BAT triggered on a precursor to the main burst of GRB 061121 ( $z=1.314$ ), allowing observations of the main burst to be made from the optical to gamma-ray bands. Many other telescopes, including Konus-Wind, XMM-Newton, ROTSE, and the Faulkes Telescope North, also observed the burst. Its main burst began 60 s after trigger, and consisted of three overlapping peaks of increasing brightness, some 63, 69 and 74 s after

trigger, as one can see in Fig. 1d. The  $\gamma$ -ray emission decayed fast after 75 s and became undetectable by the BAT beyond 140 s. The burst was also detected by Konus-Wind. The spectrum and spectral evolution of this GRB were well fit with a broken power-law. Its ‘peak’ energy appeared to increase during the rise of each flare and decreased as their flux decayed. But its isolated main strong flare at  $\sim 74$  s, as in many cases studied before, had a maximum  $E_p$  at its beginning, which decayed monotonically thereafter. After the bright burst, the X-ray emission —measured by the XRT and later also with XMM-Newton— began to follow the ‘canonical’ decay. Superimposed on the initial rapid decay from the major flare, are two smaller flares around 90 s and 125 s. The rapid decay is taken over by the plateau around 200 s and gradually breaks into a power-law decline, with an asymptotic power-law index  $\alpha = 1.59 (+0.09/-0.04)$ . The AG spectrum was well fit by an absorbed power-law with  $\Gamma = 2.07 \pm 0.06$  which slightly hardened after the AG bend/break.

**GRB 061121.** *Interpretation:* The hard mean photon spectral index  $\Gamma \sim 1.3$  and continuously decreasing  $E_p$  during the main flare are as predicted by the CB model (DD2004). The alleged increase of  $E_p$  during the rise time of the smaller flares is probably an artifact of overlapping peaks, wherein the decay of a previous flare is taken over by a new flare only near its peak time. A comparison between the observed complete X-ray light curve (Page et al. 2007) and the CB model’s fit is shown in Fig. 1c. The general trend before the onset of the synchrotron plateau is dominated by the main X-ray peak. The two smaller overlapping preceding peaks seen in the  $\gamma$ -ray light curve in Fig. 1d have been included in the fit, and so have the two late X-ray flares not intense enough to be seen in  $\gamma$ -rays. Assuming a constant density ISM, the CB model reproduces very well the observed light curve over seven orders of magnitude in intensity and five orders of magnitude in time. The model best fit to the entire X-ray light curve, yielded  $p = 2.2$ , which implies  $\beta = 1.1$  and  $\alpha = 1.6$ , in good agreement with their observed values. The CB model also correctly predicts the spectrum and spectral evolution of the X-ray emission during the rapid decline phase of the prompt emission (DDD2008a). The observed strong softening of the spectrum during the rapid-decline is in full agreement with the spectral evolution predicted by Eq. (12). When the plateau phase takes over, the spectral power-law index changes to  $\beta_X = 1.07 \pm 0.06$ , and remains in agreement with the prediction  $\beta = p/2$ . The slight hardening of the spectrum at late time to  $\beta = 0.87 \pm 0.08$  we have not predicted. It may be an artifact due to constraining the absorbing column density to a constant value as function of time during the AG phase.

**GRB 061121.** *Optical observations and a sketch of their interpretation:* The UVOT detected an optical counterpart in the white filter starting 62 s after the trigger, and subsequently in all other filters (optical and UV). The UVOT light-curve shows a prominent peak around  $t \sim 73$  s, coincident in time with the blended three main X-ray peaks, followed by a plateau phase. The complete optical light curves measured by the Swift UVOT and in

ground observations with ROTSE, FTN, CTIO and MDM follow roughly the canonical X-ray light curve which gradually bends from a shallow plateau into an asymptotic power-law decline. The peak is well fit by a SR from expanding CBs in a windy density  $\propto 1/r^2$ . The rest of the light-curve, as the canonical X-ray light curve, is well described by SR from a CB decelerating in a constant density with a spectral index gradually changing from  $\beta \sim 0.5$  above the bend frequency to  $\beta = \beta_X \sim 1$  below it, well after the the bend/break in the AG.

**GRB 050315.** *Observations:* This GRB was described/studied in detail in Vaughan et al. 2006. It is one of the first Swift GRBs with a well sampled X-ray light-curve from trigger until late time ( $\sim 10$  days). It was detected and located by BAT at 20:59:42 UT on March 15, 2005. The BAT light curve comprises two major overlapping peaks separated by about 22 seconds. Absorption features in the spectrum of its optical afterglow obtained with the Magellan telescopes indicated that its redshift is  $z \geq 1.949$  (Berger et al. 2006). The XRT began observations 80 s after the BAT trigger and continued them for 10 days, providing one of the best sampled X-ray AGs (Vaughan et al. 2006). The extrapolation of the BAT light curve into the XRT band pass showed the X-ray data to be consistent with the tail end of the decaying prompt emission. The combined light curve showed the canonical behaviour: the rapid decline ends  $\sim 300$  s after trigger, the plateau lasted for about  $10^4$  seconds, before it gradually bent into a power-law decay.

**GRB 050315.** *Interpretation:* The complete X-ray light curve of GRB 050315 is compared with the CB-model prediction in Fig. 1e. An enlarged view of the X-ray emission during the GRB and the fast decline at its end are shown in Fig. 1f. Two pulses are used in the fit. As shown, the model well reproduces the data: the exponentially decaying contributions of the two pulses describe the changing slope of the fast-decaying phase. The early ICS flares, the decay of the prompt emission and the subsequent synchrotron-dominated plateau and gradually bending light curve into a power-law decay are well reproduced by the model as shown in Figs. 1e,f.

### 5.1.2. GRBs with a single power-law afterglow

**GRB 061007.** *Broad-band observations:* The broad-band observations of this GRB were summarized and discussed by Mundell et al. (2007). The Swift BAT detected GRB 061007 on 2006 Oct 07, 10:08:08 UT. The prompt emission from GRB 061007 was also detected at MeV energies by Konus/Wind, Suzaku/WAM and RHESSI. The BAT  $\gamma$ -ray light curve shows three peaks with substantial sub-structure, and a small fourth peak around 75 s that shows long exponential decay and faint emission detectable to  $\sim 900$  s. The Swift XRT and UVOT began observing 80 s after the BAT trigger time and detected a very bright X-

ray/optical counterpart with a power-law decay identical to that of the soft  $\gamma$ -ray tail and at optical wavelengths, with a temporal slope  $\alpha_X = 1.6 \pm 0.1$  all the way to at least  $10^6$  s with no indication of any break. The best fit spectral index of the unabsorbed X-ray afterglow was  $\Gamma = 2.1 \pm 0.1$ . Robotically-triggered observations with the ground-based telescopes ROTSE and the FTS began at 26 s and 137 s, respectively, after trigger and continued (FTN) for 5.5h. Follow-up observations were performed with the VLT and Magellan-I Baade telescope. The spectral index of the unabsorbed X-ray afterglow and not extinct optical afterglow were found to be the same beyond 200 s.

**GRB 061007.** *Interpretation:* In the CB model, afterglows decaying like a single power-law are observed when the AG bend/break takes place takes place very early and is hidden under the prompt emission, or before the beginning of the observations. In the case of a constant ISM density, the decay index and the spectral index are predicted to satisfy  $\alpha = \Gamma - 1/2$  implying a decay index  $\alpha = 1.6 \pm 0.1$ . The CB model predictions for the light-curves of the X-ray and R-band afterglow of GRB 061007 are shown in Figs. 2a,b. The best fit temporal decay index is 1.6, as expected. Agreement between theory and observations is very good. The slight wiggling around the power-law decay follow, in the CB model, from density variations along the trajectory of the CBs. The reported broad-band spectral index of the unabsorbed/not-extinct afterglow,  $\beta_{OX} = 1.03$  (Mundell et al. 2007) is consistent with that predicted by the CB model (DDD2002) for a bend frequency below the optical band, as expected beyond the AG break.

**GRB 061126.** *X-ray observations:* The broad band observations of this GRB were described and discussed in detail in the framework of the fireball model by Perley et al. (2008) who found their evolution troublesome and by Gomboc et al. (2008) who found them intriguing. It was a long GRB ( $T_{90} = 191$  s) dominated by two major  $\gamma$ -ray peaks within the first 40 s, which was followed by a smooth power-law decline with a temporal index  $\alpha \sim 1.3$ . Due to an Earth limb constraint, Swift slewed to the burst only after 23 minutes and followed its X-ray AG from 26 minutes to 20 days after burst. Its X-ray AG showed roughly a power-law decline with the same power-law index  $\alpha_X \sim 1.3$ , with marginal evidence for steeper early and very late time-declines with  $\alpha \sim 2$ . Its unabsorbed X-ray afterglow had a best fit spectral index  $\beta_X = 0.94 \pm 0.05$ .

**GRB 061126.** *Optical observations:* In the optical band GRB 061126 was one of the brightest Swift GRBs. Its optical emission was detected by RAPTOR during the  $\gamma$ -ray emission 21 s after the BAT trigger, and its early decline was followed also by the PAIRITEL, NMSU, KAIT Super Lotis and FTN robotic telescopes. Observations continued with several large telescopes. The observations were summarized and discussed in Perley et al. 2008 and in Gomboc et al. 2008. The initial power-law decay of the optical AG with  $\alpha 1.5$  changed to

a shallower decline approximately 1000 s after the burst which steepened about 1.5 day after the burst. The last optical data point ( $0.52 \pm 0.05 \mu\text{Jy}$ ) obtained with Gemini North at 15 days after burst (Gomboc et al. 2008) was slightly dimmer than the host galaxy at redshift  $z = 1.16$  (Perley et al. 2008) whose R magnitude  $24.10 \pm 0.11$  ( $0.70 \pm 0.07 \mu\text{Jy}$ ) was measured with the Keck telescope 54 days after burst. After correcting for Galactic extinction and estimated extinction in the host galaxy, its observed early time optical emission had  $\beta = 1. \pm 0.1$  and showed a strong colour evolution towards  $\beta_O \sim 0.4 - 0.5$  around 2000s. The late time index was typically  $\beta_O = 0.95 \pm 0.10$ , consistent with  $\beta_O = \beta_X$ .

**GRB 080319B** *Observations:* This GRB was detected by Swift (Racusin et al. 2008b), Integral (Beckmann et al. 2008) and Konus-Wind (Golenetskii et al. 2008) satellites. It lasted  $\sim 60$  s. It had the largest energy fluence, so far, of a long GRB. Three robotic ground telescopes detected its extremely intensive optical light emission (Karpov et al. 2008, Cwiok et al. 2008, Wozniak et al. 2008) before the Swift alert, and saw it brightening to a visual peak magnitude 5.4, visible to the naked eye, some 18 s after the start of the burst. Swift XRT slewed to the GRB position within 65 s and followed its power-law declining X-ray light curve for the first 15 days. Swift’s prompt alert sent to the world’s telescopes triggered many follow-up observations including Spectral measurements with the VLT (Vreeswijk, et al. 2008) and Hobby-Eberly telescope (Cucchiara et al. 2008) determined the GRB’s redshift to be  $z = 0.937$ . Its X-ray light curve measured with the Swift XRT ([http://www.swift.ac.uk/xrt\\_curves](http://www.swift.ac.uk/xrt_curves) Evans et al. 2007) is shown in Fig. 2e and its combined R-band and V band normalized to the R-band light curve reported in GCNs (see e.g., Bloom et al. 2008 and references therein) is shown in Fig. 2f

**GRB 080319B.** *Interpretation:* In the CB model the ICS spectrum of the scattered glory’s photons is an exponential cut-off power-law with a spectral index,  $\Gamma \approx 1$ , cut-off energy  $\approx E_p$ , and a power-law tail (see Eq. (4) in agreement with the spectral index,  $\Gamma = 1.01 \pm 0.02$  in the 15-350 keV range, reported by the Swift BAT team (Racusin et al. 2008b), and with the Band function fit to the broader 20 keV - 7 MeV energy range, reported by the Konus-Wind team (Golenetskii et al. 2008).

In Fig. 2e we compare the X-ray light curve of GRB 080319B measured with the Swift XRT and its CB model description (Eq. (26) assuming a constant ISM density and approximating the result by a single dominant or average CB. The best-fit parameters are  $\gamma_0 \theta = 0.07$ ,  $t_b = 70\text{s}$  and  $p = 2.08$ , yielding an approximate power-law decline beyond  $t_b$  with  $\alpha_X = 1.54$ . The fit is quite good except around  $4 \times 10^4$  s, where it is poorly sampled. As expected (DDD 2008a) for very luminous GRBs, no AG break is observed. The temporal index,  $\alpha_X = \Gamma_X - 1/2 = 1.42 \pm 0.07$ , predicted from the late-time photon spectral index,  $\Gamma_X = 1.92 \pm 0.07$ , reported by the Swift XRT team (Racusin et al. 2008c), is in agreement

with the best-fit temporal index. At  $t \sim 4 \times 10^4$ s, the data lie below the fit. If not a statistical fluctuation, this may be due to a failure of the constant-density approximation, not surprising at this level of precision. Better optical data in the same time domain may resolve this question.

GRB 080319B started with a succession of prompt  $\gamma$ -ray pulses, but the XRT observations started too late to see their X-ray counterparts. Their counterparts were seen at and optical frequencies. Even though the optical pulses are SR-generated, their expected time dependence (Eq. 33) is akin to that of the  $\gamma$ -ray pulses. The CB model optical light-curve of GRB 080319 shown in of Fig. 2f was obtained by fitting each of the three early pulses observed by the TORTORA instrument (Karpov et al. 2008). The later-time AG, given by Eq.(26) beyond  $t_b \sim 70$  s, is essentially a power-law decline, insensitive to  $\gamma_0 \theta \ll 1$  and  $t_b < 70$ s but sensitive to  $\beta_O$ . In the CB model, the index  $\beta$  is  $\sim 0.5$  below and  $\sim 1.1$  above the ‘bend frequency’,  $\nu_b(t) \propto \sqrt{n} \gamma^3 \delta$  which usually ‘crosses’ the optical band within  $t \sim 1$  day, so that  $\beta_O \approx \beta_X$  thereafter. Our best fit to the optical AG results in  $\alpha_{opt} = 1.40 \pm 0.04$ , which implies a late-time  $\beta_{opt} \approx 0.90$ , consistent with the late time expectation. So far no late-time spectral information is available to verify this prediction.

When a CB crosses a density enhancement,  $\nu_b$  increases due the sudden increase in  $n$  and the delay in the consequent CB deceleration. The bend frequency may cross the optical band ‘backwards’: from above, to below it. Such a spectral evolution may have been observed some 5000 s after the onset of the burst (Bloom et al. 2008). The spectral analysis of the UNLV GRB group (Zhang et al. 2008) shows a decreased  $\beta_X = 0.70 \pm 0.05$  around that time. The expected  $\beta_{opt} \approx \beta_X - 0.5 = 0.2 \pm 0.05$  at that time is consistent with the reported (Bloom et al. 2008) spectral evolution around 5000 s after burst.

### 5.1.3. GRBs with semi-canonical X-ray light curve

**GRBs 060211A, 061110A, 051021B, 080307, 080303, 070220.** Observations and Interpretation: These GRBs detected by the Swift BAT and followed up by the Swift XRT essentially GRBs with canonical X-ray light curves, except that their exponentially declining phase at the end of the prompt emission changed into a slower power-law decline before they entered the plateau phase of canonical light curves. Their X-ray light curves, extracted from the Swift/XRT GRB light curve repository (Evans et al. 2007, [http://www.swift.ac.uk/xrt\\_curves/docs.php](http://www.swift.ac.uk/xrt_curves/docs.php)) are shown in Figs. 3a-f together with their CB model description. In the CB model the exponential decline of the prompt ICS emission as given by Eq. (12) is taken over by the SR emission from the CBs, which, in a windy circumburst environment, decays like a power-law,  $F_\nu \sim t^{-(1+\beta_X)} \nu^{-\beta_X}$  (see Eq. (33)). This

take over by SR is accompanied by a sudden hardening of the AG spectrum to the ordinary SR spectrum,  $\sim \nu^{-\beta_X}$  with  $\beta_X \sim 1.1$ . This power-law temporal decay changes into the canonical plateau phase when the CBs enter the constant ISM density. In the case of GRB 070220, the fast asymptotic decline, was well fit assuming an isothermal sphere density profile,  $n \propto 1/(r^2+r_c^2)$ , as in the cases shown in Figs. 6,7.

#### 5.1.4. GRBs with large X-ray flares during the early X-ray afterglow

**GRB 060526.** *X-ray observations:* This GRB was detected by Swift’s BAT at 16:28:30 UT on May 26, 2006 (Campana et al. 2006a). The XRT began observing the field 73 s after the BAT trigger. The burst started with a  $\gamma$ -ray emission episode lasting 18 s. The GRB was thereafter quiet for about 200 s, and then emitted two additional pulses which lasted about 50 s and were also coincident with strong X-ray flares between 220 s and 270 s after trigger. The XRT followed the X-ray emission for 6 days until it faded into the background. The entire XRT light curve is shown in Fig. 3a. It has the ‘canonical behaviour’ of many Swift GRBs, and two superimposed early time large flares.

**GRB 060526.** *Optical observations:* The observations of the optical emission from GRB 060526 are summarized and discussed in Dai et al. 2007 and Khamitov et al. 2006. They were started as early as 36.2 s after the BAT trigger by the Watcher 40cm robotic telescope, in South Africa (French & Jelinek 2006). It saw the AG at a very bright 15th magnitude. The UVOT on Swift detected its optical AG 81 s after the BAT trigger (Campana et al. 2006a). The burst was followed up with UVOT and ground-based telescopes by several groups. Spectra obtained with the Magellan/Clay telescope indicated a redshift of  $z = 3.21$  (Berger & Gladders 2006). Its R-band light curve obtained with the MDM and PROMPT telescopes at Cerro Tollolo, and with other telescopes, is shown in Fig. 3b (Dai et al. 2007 and references therein). It can be seen in Figs. 3a,3c that apart for the superimposed large early-time X-ray flares which are not present in the optical light curve and late mini flares, the X-ray light curve and the well sampled R-band light curve show, roughly an achromatic behaviour.

**GRB 060526.** *Interpretation:* The entire X-ray light-curve and its CB-model’s fit are shown in Fig. 3a. Three ICS pulses were used in the fits of the early time emission, although the third pulse may well be a superposition of two unresolved pulses. The pulse shape and the spectral evolution of the the last two large flares are typical of ICS flares (DDD2008a). Their coincidence in time with the late  $\gamma$ -ray peaks and the absence of corresponding peaks in the optical UVOT light curve, and their spectral evolution support their interpretation as part of the prompt GRB emission, continuing up to relatively large emission times partly because of the large redshift of the burst source which stretches observer time by a relatively

large factor,  $z+1 = 4.21$ . A zoom-in on these two ICS X-ray flares is shown in Fig. 3b. The decay of the prompt emission is dominated by the decay of the last pulse. Figs. 3a,b,c demonstrate that the early ICS flares, the decay of the prompt emission the subsequent synchrotron-dominated plateau and its gradual bending light curve into a power-law decay are all well reproduced by the CB model. In Fig. 3d we show the theoretical R-band light curve obtained with the parameters which were fitted to the SR X-ray light curve. Since the bending frequency during the steepening phase is below the R band, the temporal decay of the R-band light curve practically coincides with that of the X-ray light curve. Both the X-ray and the late time optical light curve are bumpy, which may be caused by mini flares and/or density inhomogeneities, which we have not tried to fit. The apparent steeper decay of the optical AG beyond 1 day may be the decline following a flare or a transition into the galactic halo with a declining density like  $r^2$ .

**GRB 060206.** *Observations:* This GRB triggered the Swift’s BAT on February 6, 2006 at 04:46:53 UT (Morris et al. 2006). Its  $\gamma$ -ray emission lasted only 6 s. The XRT started its observations 80 s after the BAT trigger. Despite its initial poor time sampling, it detected an X-ray decline after 1/2 hour and a strong rebrightening after one hour, after which its follow up was nearly continuous for some 20 days. The bright optical AG of GRB was detected by Swift at  $V = 16.7$  about a minute after the burst. RAPTOR started observations 48.1 minutes after the BAT trigger and reported that after an initial fading, the AG rebrightened 1h after the burst by  $\sim 1$  magnitude within a couple of minutes (Wozniak et al. 2006). Many observatories followed the bright optical AG (Stanek et al. 2007 and references therein), and Fynbo et al. (2006a) carried out spectral observations to determine its large redshift,  $z = 4.05$ , later confirmed by other groups. The RAPTOR data clearly shows that the rebrightening was due to a couple of flares (Wozniak et al. 2006). Similar “anomalous” rebrightening of the optical afterglow was seen in some other bursts (Stanek et al. 2007) .

**GRB 060206.** *Interpretation:* In Fig. 6a,b we compare the observations of the X-ray and R-band light curves with the CB-model fits. Superimposed on the plateau phase are two strong flares beginning around 1 h after trigger. The coincidence in time of the X-ray and optical flares and the absence of any evidence for the typical ICS strong spectral evolution, suggest that these two flares are SR flares due to encounter with a density jump such as at the boundary of a superbubble created by the star formation region.. In Fig. 6c we compare the observed light curve of these two flares in the R-band and their CB model description via Eq. (33). The figures show that the agreement is very good and that there is nothing ‘anomalous’ in the X-ray and optical data of GRB 060206. Instead, their prominent structures are well described and precisely related by their CB-model’s understanding in terms of a sudden jump in the ISM density.

### 5.1.5. GRBs with chromatic ‘afterglows’

**GRB 050820A.** *Broad Band Observations:* This GRB is one of the Swift GRBs with best-sampled broadband data. These data are summarized and discussed in detail in Cenko et al. 2006. The burst was detected and observed by Swift and Konus-Wind. Its  $\gamma$ -ray emission was preceded by a soft precursor pulse some 200 s before the main burst which lasted some 350 s and consisted of 5 well separated major peaks, with clear spectral evolution from hard-to-soft within each peak. The main peak observed by Swift during 217 << 241, and the time integrated photon spectrum over the entire burst were well fit with a cut-off power-law with a photon index  $\Gamma = 1.07 \pm 0.06$  and  $\Gamma = 1.12 \pm 0.15$  (and  $E_p \sim 367$  keV), respectively. The Swift XRT began observations began 88 s after the burst trigger and followed its X-ray light curve until 44 days after burst (see Fig. 5a). The measured mean photon index, of the unabsorbed emission in the 0.3-15 keV band during the prompt emission phase was  $\Gamma = 1.06 \pm 0.04$  ( $\beta_X = 0.06 \pm 0.04$ ) and  $\Gamma = 2.06 \pm 0.07$  ( $\beta_X = 1.06 \pm 0.07$ ) during the afterglow phase (Evans et al. 2007).

The prompt optical emission was measured by the robotic telescope RAPTOR beginning 18 s after the BAT trigger. The Swift UVOT began observations 80 s after the BAT trigger but became inoperable when Swift entered the South Atlantic Anomaly approximately 240 s after the BAT trigger. The automated Palomar 60-inch telescope, started observations 206s after the BAT trigger and continued follow-up until late time. Later measurements were made by Turkish Russian 1.5 m telescope. Late time images were taken with the 9.2 m Hobby-Eberly Telescope (HET) and with the Hubble Space Telescope (HST) until 37 days after burst. The R-band light curve is shown in Fig. 5b. Ignoring host reddening, and correcting for Galactic extinction,  $E(B-V)=0.044$ , in the burst direction, the fitted spectral index (Cenko et al. 2006) in the optical band during the prompt emission was  $\beta_O=0.57 \pm 0.06$  and steepened to  $\beta_O=0.77 \pm 0.08$  within the first day. While the optical spectrum appeared steeper later on, the poor fit quality precluded a reliable value. Figs. 5a and 5b demonstrate a very chromatic behaviour of the X-ray and the optical light curves during the prompt and afterglow phases.

**GRB 050820A.** *Interpretation.:* The pulse shape of the prompt-emission  $\gamma$ /X-ray peaks and their spectral index agree well with those predicted by ICS of glory light, The CB model fit to the entire XRT light curve is shown in Fig. 5a. The early time light curve is well described by the ICS X-ray counterparts of the prompt  $\gamma$ -ray peaks: The very early time XRT light curve is the tail of the precursor pulse, the next pulse is the X-ray counterpart of the first ICS  $\gamma$ -ray pulse around 220 s. The ICS peaks are superimposed on a canonical SR afterglow with a bend/break around 1000s. The X-ray peak around 5000s is interpreted as a flare due to a density bump superimposed on a canonical AG.

While the prompt  $\gamma$ -ray and X-ray emission is dominated by the ICS of glory light by CBs, which yields  $\beta \sim 0$ , the optical emission is dominated by their SR emission as summarized in Eq. (33) with the typical  $\beta \sim 0.5$ , as observed. The different radiation mechanisms are responsible for the chromatic behaviour of the prompt emission.

Although both the X-ray AG and the optical AG are dominated by SR, the optical AG evolves differently than the X-ray AG because of its dependence on the bend frequency which depends on the ISM density and on the Lorentz factor of the decelerating CB. Consequently, the early time optical and X-ray AGs are chromatic until the bend frequency crosses well below the optical band and then,  $\beta_O = \beta_X$ . This is shown in Figs. 5a and 5b. The CB model R-band light curve shown in Fig. 5b was calculated with  $\beta_O = 0.77$  and the best fit parameters of the X-ray afterglow shown in Fig. 5a. The calculated light curves did not include late time flares in order not to obscure the chromatic behaviour of the underlying smooth afterglows.

**GRB 060418.** *Broad Band Observations:* This GRB was discussed in detail in Molinari et al. 2007. Its  $\gamma$ -ray emission was detected and observed by the Swift BAT and by Konus-Wind. The BAT light curve showed three overlapping peaks at 10 s, 18 s and 27 s and a bump which coincided with an X-ray flare at 128 s after trigger. The Swift XRT started observing the GRB 78 s after the BAT trigger. The XRT light curve shows a prominent flaring activity superimposed on a smooth afterglow decay. A prominent peak, also visible as a bump in the BAT data, was observed at about 128 s after trigger. The REM robotic telescope began observing GRB 060418 64 s after the burst trigger in the z’JHK-band and followed it down to the sensitivity limits. The UVO/NIR AG was also detected by the Swift UVOT, by one of the 16-inch PROMPT telescopes at CTIO and by the robotic telescope FRAM (part of the Pierre Auger Observatory). The NIR/optical AG was also followed up with the 1.3 m telescope at CTIO beginning  $\sim 1$  h post-trigger, and with the PAIRITEL 1.3 m telescope staring 2.53 h after the GRB trigger. The UVO/NIR light curves show a very chromatic initial behaviour compared to the XRT light curve (Figs. 5c and 5d). The NIR AG rises until reaching a maximum around 130 s after trigger and then gradually changes to a power-law decline shallower than that of the X-ray AG, with a weak flare superimposed on it around 5 ks, which roughly coincides in time with a strong X-ray flaring activity.

**GRB 060418.** *Interpretation:* The XRT light curve was fit by the tail of the prompt ICS emission and an ICS flare around 128 s which was later taken over by the SR afterglow of a CB moving in a constant density ISM (Fig. 5c). The bend/break of the SR afterglow is hidden under the tail of the X-ray flare at 128 s. The H-band light curve, shown in Fig. 5d, was calculated using Eq. (33) with an early time unabsorbed  $\beta_O = 0.5$  and an ejection time,  $t_i = 26$  s, coincident with the beginning time of the major  $\gamma$ -ray peak. No attempt was made

to model the flaring activity around 5ks.

**GRB 071010A.** *Broad Band Observations:* This GRB at redshift  $z=0.985$  was discussed in detail by Covino et al. (2008). It was a 6 s long single peak GRB detected by the Swift BAT. Swift did not slew to this GRB because its automatic slewing to GRBs was temporarily disabled. Swift XRT began observing the GRB 071010A only 34 ks after the BAT trigger and followed it until 550 ks after trigger. The XRT light curve (Fig. 5e) shows a wide flare peaking around 60 ks and followed by a power-law decay with an index  $\sim 1.6 \pm 0.3$ . The early optical/NIR emission of GRB 071010A was observed by the TAROT, REM and the 2.2 m MPI/ESO telescopes. Follow-up NIR observations were carried out with Gemini-North, TNG and the NTT. The afterglow was observed a few hours after the GRB with the Keck-I and Sampurnan telescopes and with NOT and VLT. The NIR/Optical light-curve shows an initial rising phase with a maximum at about 7 min, a smooth decay interrupted by a flare about 0.6 d visible in both the optical/NIR and X-rays (Figs. 5e and 5f). The NIR/optical spectrum was modeled by a power-law with an SMC-like extinction law with a best fit  $E(B - V) = 0.21$ . The reported unabsorbed late index was  $\beta_O = 1.26 \pm 0.26$ .

**GRB 071010A.** *interpretation:* The NIR/Optical light curves were interpreted as the SR radiation from a CB ejected into a windy  $1/r^2$  density profile, as given by Eq. (33) until taken over by a constant density ISM, with a a standard wide flare superimposed on the AG around 0.6 d. The late XRT light curve was calculated with the same parameters except for  $\beta_X = 1.1$ .

### 5.1.6. GRBs with very fast decaying late afterglows

Figs. 6 and 7 show well sampled XRT light curves of 12 GRBs, 050318, 050326, 050814, 051008, 061019, 060807, 060813, 070306, 070419B, 070420, 070521 and 080207, with a late decay more rapid than the canonical  $t^{-1.6}$  decline of the AG of CBs decelerating in a constant density ISM. In the CB model, such a fast decline, is produced by a fast declining ISM density or by the tail of a late flare. We have found that all Swift GRBs with a well sampled fast declining X-ray light curves can be reproduced by either an asymptotic  $n \sim 1/r^2$  density profile or a tail of a late flare, as demonstrated in Figs. 6 and 7. Such an asymptotic density decline is typical of isothermal spheres where,  $n(r) = n_0/[1 + (r/r_c)^2]$ , which well represent the ISM density profile in galactic bulges of spiral galaxies, in elliptical galaxies and after bumps created by stellar winds (whose crossing by CBs presumably generates by SR the late AG flares). The CB model predicts that for  $r \gg r_c$ , the AG declines like  $F_\nu \propto t^{-(1+\beta)} \nu^{-\beta}$ , i.e., with  $\alpha = \beta + 1 = \Gamma_{SR} \sim 2.1$ . In some GRBs the transition from  $\alpha = \Gamma - 1/2 \sim 1.6$  for  $r \ll r_c$ , to,  $\alpha = \Gamma \sim 2.1$  for  $r \gg r_c$ , probably have been misinterpreted as a late achromatic

jet break of the fireball model (e.g., Dai et al. 2008, Racusin et al. 2008a).

### 5.1.7. GRBs with complex chromatic light curves

**GRB 050319. *Observations:*** The Swift BAT, XRT and UVOT observations of this GRB were discussed in detail in Cusumano et al. 2006a and Mason et al. 2006. A reanalysis of the BAT data showed that its onset was  $\sim 135$  s before the trigger time reported by Krimm et al. (2005). The XRT began its observations 90 s after the BAT trigger, continuing them for 28 days (Cusumano et al. 2006a). The *gamma*-ray light-curve shows two strong peaks. The X-ray light curve had the canonical behaviour: an early fast decline which extrapolated well to the low-energy tail of the last prompt  $\gamma$ -ray pulse at around 137 s after the onset of the GRB. After  $\sim 400$  s, the fast decline was overtaken by a plateau which gradually bent into a power-law decline after  $\sim 10^4$  s. The spectral index of the afterglow,  $\beta_X = 0.73 \pm 0.05$ , and its asymptotic temporal decline index,  $\alpha = 1.14 \pm 0.2$ , (Cusumano et al. 2006a) well satisfy the relation  $\alpha = \beta + 1/2$  but both were obtained by correcting only for Galactic absorption and no IGM and host absorption.

**GRB 050319. *Interpretation:*** A CB model fit to the complete X-ray light curve is shown in Figs. 8a. Two pulses are used in the early ICS phase. The early ICS flares, the decay of the prompt emission and the subsequent synchrotron-dominated plateau and gradually bending light curve into a power-law decay are well reproduced by the model.

**GRB 050319. *UVO observations:*** The UVOT detected an optical counterpart in the initial White filter30 observation, starting 62 s after the trigger, and subsequently in all other filters (optical and UV). Swift’s UVOT which followed the typical sequence for GRB observations. was able to observe the UVO emission 140 s after its detection by the BAT. It was also observed by ground-based robotic telescopes RAPTOR (Wozniak et al. 2005), and ROTSE III (Quimby et al. 2006a) just 27.1 s after the Swift trigger. The optical AG was followed later with a number of ground based telescopes (Huang et al. 2006 and references therein). An absorption redshift,  $z = 3.24$ , was reported from observations with the Nordic Optical Telescope (Jakobsson et al. 2006). The afterglow of this GRB is highly chromatic with no apparent correlated behaviour between its X-ray and optical emission, as can be seen from Figs. 2a,2b.

**GRB 050319. *Interpretation of UVO observations:*** The early time optical light curve was fit by SR emission from two separate CBs implied by the first two strong  $\gamma$ -ray peaks. The late X-ray and optical AG were calculated with the same deceleration parameters. The complex optical light curve is reproduced well, as shown in Fig. 8b.

**GRB 060605.** *Broad band observations:* This GRB at redshift  $z = 3.773$  was studied and discussed by Ferrero et al. 2008. It was a long and relatively faint gamma-ray burst with a duration of about 20 sec detected by the Swift BAT. Its BAT light curve showed two overlapping peaks. The Swift XRT which began taking data 93 seconds after the BAT trigger and followed it until 200 ks. The XRT light curve shows a canonical behaviour with a flare around 265 s after trigger superimposed on a shallow plateau phase which began  $\sim 200$  s after the BAT trigger and changed into an asymptotic power-law decline beyond 8 ks (Fig. 8c). The best fit spectral index of the unabsorbed spectrum in the X-ray band was  $\beta_X = 1.06 \pm 0.16$ . The UVOT which began observations of GRB field 97 s after the BAT trigger detected and localized its fading afterglow. Follow up observations in the UVONIR bands were carried out also with ROTSEIIIa which began 48 s after trigger and with the VATT, RTT, TNG and the Kitt Peak 2.1 m telescopes. Fig. 8d shows the recalibrated  $R_c$  band light curve from these observations (Ferrero et al. 2008). In contrast with the XRT light curve, it shows a chromatic early rise with a ‘broken’ power-law decay. The XUVONIR data show a spectral evolution at early time from  $\beta_{OX} 0.8 \pm 0.05$  at 0.07 d, to a spectral index  $\beta_{OX} 1.02 \pm 0.02 \approx \beta_X$  at 0.43 d.

**GRB 060605.** *Interpretation:* The XRT light curve was fit with a canonical CB model X-ray light curve (Fig. 8c), which begins with the tail of the fast decline of the prompt ICS emission, and is taken over by the synchrotron emission in a constant density environment which changes to an  $1/r^2$  beyond 8 ks. The bump around 250 s was interpreted as an SR flare superimposed on the smooth canonical AG. The corresponding R-band light curve, shown in Fig. 8d, was generated using Eq. (33) with the fit parameters of the X-ray flare and the canonical  $\beta_O = 0.5$  for an early optical emission, until it was taken by the SR emission in the density used in the CB model description of the late X-ray afterglow.

**GRB 060607A.** *Broad band observations:*

This GRB at redshift  $z = 3.082$  was studied by Molinari et al. (2007), Nysewander et al. (2007) and Ziaepour et al. (2008). The Swift XRT began observing it 73.6 sec after the BAT trigger. Its complex X-ray light curve, like that of quite a few other GRBs, was dominated by strong flaring activity. As shown in Fig. 8c) the XRT light curve exhibits three early time flares peaking at approximately 97 sec, 175 sec, and 263 sec after the BAT trigger and a continuing weaker flaring activity superposed on a decaying continuum. The UVOT began to observe the bright optical afterglow of this GRB 75 seconds after the BAT trigger. The REM telescope began NIR observations of GRB 060607A 59 s after the BAT trigger. It detected a brightening smooth light curve which peaked around  $\sim 155$  s and decayed like a power-law afterward interrupted by flaring activity beyond 1000 s. REM followed the decay for 20 ks down to its sensitivity limit. Four 0.4-m PROMPT telescopes began observing

the afterglow of GRB 060607A 44 s after trigger and measured its UVO light curves until 20 ks after trigger which showed the same behaviour as its NIR light curve (Nysewander et al. 2007).

**GRB 060607A.** *Interpretation:* The complex X-ray light curve of this GRB, like that of quite a few other GRBs, which is dominated by a strong flaring activity, as can be seen in Fig. 8e, was fit with 6 flares superimposed on the AG of a fitted, single, dominant CB. This fit, which can be improved by splitting the last flare into two, is a very rough description ( $\chi^2/dof = 4.9$  for 440 *dof*), not a proof of the quality of a prediction. Moreover, in cases with such a prominent flaring activity, the mean photon spectral index of the AG data is an average between the typical index of flares,  $\Gamma = 1.5$ , and that of synchrotron AG,  $\Gamma = 2$ , i.e., an average significantly smaller than that of the synchrotron AG. Thus, we do not expect such a labyrinthine AG to satisfy the CB-model spectral-index relations, Eqs. (28,29). The early UVONIR CB model light curves, as demonstrated in Fig. 8f for the H band, is well described by the smooth SR afterglow of a single CB moving in a wind environment, as given by Eq. (33). We did not try to fit the superimposed weak flaring activity on the smooth decline, which is probably due to a bumpy wind environment..

#### 5.1.8. XRF060218

**XRF060218/SN2006aj.** *Broad Band Observations:* This XRF/SN pair provides one of the best testing grounds of theories (De R'jula 2008) given its proximity, which resulted in very good sampling and statistics (see, e.g., Campana et al. 2006b, Pian et al. 2006, Soderberg et al. 2006, Mirabal et al. 2006, Modjaz et al. 2006, Sollerman et al. 2006, Ferrero et al. 2006). The XRF was detected with the Swift's BAT on 2006 February 18, at 03:34:30 UT (Cusumano et al. 2006b). The XRT and UVOT detected the XRF and began taking data 152 s after the BAT trigger. The XRT and UVOT detection led to its precise localization, determination of its redshift,  $z = 0.033$ , (Mirabal et al. 2006) and the discovery of its association with a supernova, SN2006aj (Nousek et al. 2006). The BAT data lasted only 300 s, beginning 159 s after trigger, with most of the emission below 50 keV (Campana et al. 2006b, Liang et al. 2006). The total isotropic equivalent  $\gamma$ -ray energy was  $E_{\text{iso}} \sim 0.8 \times 10^{49}$  erg and the spectral peak energy,  $E_p$ , strongly evolved with time from  $\sim 54$  keV at the beginning of observations by the BAT down to  $< 5$  keV 300s later. The X-ray light curve of 060218 (Campana et al. 2006b) was followed up with the XRT until nearly  $1.1 \times 10^6$  s after burst. It showed the canonical behaviour of X-ray light curves of XRFs and GRBs, except that the prompt X-ray emission was stretched in time and lasted more than 2000 s. The prompt emission ended with a fast temporal decline and a rapid spectral softening (Fig. ??) that

was overtaken around 10 ks by an ordinary power-law decaying AG. Follow-up observations with the UVOT and ground based telescopes showed a very chromatic UVONIR AG with a long brightening phase with a peak between 30 and 60 ks which changed into a fast decline and was taken over around 2 d after burst by the rising light curve of SN2006aj (Marshall et al. 2006, Campana et al. 2006b, Pian et al. 2006, Mirabal et al. 2006, Sollerman et al. 2006, Ferrero et al. 2006). Spectral measurements of the the light of SN2006aj showed negligible additional extinction, (Pian et al. 2006, Guenther et al. 2006) beyond the Galactic extinction,  $E(B-V)=0.13$ , along the line of sight to SN2006aj.

**XRF060218/SN2006aj.** *Interpretation:* The spectral energy distribution measured with the Swift BAT and XRT was parametrized (e.g., Campana et al. 2006b, Liang et al. 2006) as the sum of a black body emission with a time-declining temperature from a sphere with time-growing radius and a cut-off power-law SR with time-dependent amplitude and cutoff energy. The alleged black body emission was interpreted as the result of shock break-out from the stellar envelope into the stellar wind of the progenitor star of the core collapse SN2006aj (Campana et al. 2006b, Blustin 2007, Waxman, Meszaros & Campana 2007). From this interpretation, a delay of  $\leq 4$  ks between the SN and the GRB start was concluded. However, a flexible parametrization is far from providing convincing evidence for the underlying model. Fortunately, the fast declining temperature deduced from the broad band XUV observations allows a conclusive test of the alleged black body emission from a shock-breakout, independent of the complex parametrization of the X-ray light curve: The early optical emission of GRB 060218 (the first  $10^5$  s after the BAT trigger) that was measured by the UVOT, and has been interpreted as a black body emission associated with the shock-breakout, required an intrinsic reddening of  $E(B-V)=0.20 \pm 0.03$  (assuming a Small Magellanic Cloud reddening law) in addition to a Galactic reddening of  $E(B-V)=0.14$  (Campana et al. 2006b, Ghisellini et al. 2007) in order to be consistent with a black body spectrum. However, such an host extinction is inconsistent with the negligible extra-Galactic extinction which was measured from the spectrum of SN2008aj by various authors (e.g., Pian et al. 2006, Guenther et al. 2006). With a negligible reddening in the host Galaxy, the ratio between the measured fluxes with the V and UVW2 filters of the Swift UVOT and dereddened with the Galactic  $E(B-V)=0.13$ , is different by nearly a factor 10 (!) from an expected  $F_\nu \propto \nu^2$  behaviour in the Rayleigh-Jeans part of a black body spectrum. Moreover, the observed flux ratio between these two bands is time-dependent and increases by a factor  $\sim 2.5$  between 2 ks and 20 ks after burst, while it should be constant as long as the optical band stays in the Rayleigh-Jeans part of the black body spectrum. Also the alleged cut-off power-law SR component in the X-ray band, is inconsistent with SR origin: Using the alleged SR contribution (Campana et al. 2006) to the prompt X-ray emission and assuming  $F_\nu \sim \nu^{-\beta_{OX}}$  with  $\beta_{OX} \geq 0.8$ ), as usually observed in ordinary XRFs and GRBs, the expected SR contribution

to the UVO band is larger by three orders of magnitude than the dereddened UVO fluxes measured with the UVOT at the same early time  $t < 1$  ks.

The light curves of XRF060218/SN2006aj measured with the Swift’s UVOT filters are particularly interesting. Not only they provide evidence that the XRF was produced in the explosion of SN2006aj, but, together with the BAT and XRT light curves, they confirm the CB-model interpretation of the broad band emission at all times. Prior to the dominance of the associated supernova’s radiation, the UVO light curves show wide peaks whose peak-time shifts from  $t_{peak} \approx 30$  ks at  $\lambda \sim 188$  nm to  $t_{peak} \approx 50$  ks at  $\lambda \sim 544$  nm, and their peak-energy flux decreases with energy (Fig. 9b). In the CB model these are the predicted properties of a single peak generated by a single CB as it Compton up-scatters glory’s light. In the CB model the prompt  $\gamma$ -ray and X-ray emission of ordinary GRBs is dominated by ICS while the optical emission is dominated by SR. However, in low-luminosity XRFs also the optical emission is dominated by ICS of glory light. The dominant radiation mechanism in the prompt emission can actually be identified, using the different spectral and temporal shapes of the ICS and SR emissions: while the early unabsorbed SR contribution has a spectral energy density  $F_\nu \propto \nu^{-0.6}$ , the ICS has  $F_\nu \propto e^{-E/E_p(t)}$  and satisfies the  $E t^2$  law. In order to test whether the prompt X-ray peak around 1000 s and the UVOT peaks between 30 and 50 ks belong to the same ICS pulse, we have plotted the energy fluxes between 5 ks and 150 ks which were measured with the UVOT filters, dereddened for Galactic extinction  $E(B-V)=0.14$  (Campana et al. 2006b) and scaled by the  $E t^2$  law, together with the unabsorbed energy flux in the 0.3-10 keV band of the prompt X-ray pulse which was measured with the XRT (Campana et al. 2006b). Each dereddened energy flux in the UVOT filters at time  $t$  was converted to energy flux density using the UVOT energy band width,  $\Delta E = h \nu \Delta \lambda / \lambda^2$  with  $\Delta \lambda = 75, 98, 88, 70, 51$  and  $76$  nm, being the FWHM of the V, B, U, UVW1, UVM1 and UVW2 filters of the Swift UVOT, with central wave lengths,  $\lambda = 544$  nm,  $439$  nm,  $345$  nm,  $251$  nm,  $217$  nm, and  $188$  nm respectively. These energy flux densities were multiplied by the XRT band width and plotted at time  $t (\nu/\nu_x)^{0.5}$  where  $h \nu_x = 5.15$  keV is the central energy of the 0.3-10 keV band. As can be seen from Fig. 9c, the XRT and UVO data around peak times seem to satisfy quite well the  $E t^2$  law. Note in particular the very large differences between the X-ray pulse shape, peak time and peak energy flux (PEF) in the Swift XUVOT bands before applying the  $E t^2$  law to the data. In Tables 3,4 and Figs. 10a,b we further demonstrate this point for the observed peak-energy flux (PEF) and peak-times in the different UVOT filters. The observed small deviations from the  $E t^2$  law in Fig. 9b may be due to its approximate nature, our rough spectral integrations, a significant SR contribution to the UVOT light curves and a non negligible contribution from the SN light at a relatively early time to the VBU light curves. In fact, there is a strong indication for a significant SR contribution to the early time UVO light curves: The spectrum obtained from

the dereddened UVOT data at early time,  $t < 5$  ks, is consistent either with SR spectrum below the frequency bend,  $F_\nu \sim \nu^{-0.6}$ . or with the  $E t^2$  law applied to the early X-ray data. This is demonstrated in Figs. 9c,d. In Fig.9c we have plotted  $\nu^{0.6} F_\nu$  for  $t < 5$  ks obtained from the UVOT dereddened data in Campana et al. 2006b. As demonstrated in Fig. 9c, the UVOT data plotted this way follow a universal line. A black body  $F_\nu \sim \nu^2$  multiplied by  $\nu^{0.6}$  would have produced e.g., two lines for the V and UVW2 bands that are separated by a factor  $\sim 14$ , entirely inconsistent with the UVOT data which is plotted in Fig. 9c.

From the above ‘model-independent’ analysis of the data on the early time emission from XRF 060218, we have concluded that the observed early-time X-ray and UVO light curves are consistent with ICS of glory light by a jet breaking out from SN2006aj, while they are inconsistent with a thermal black body radiation from a shock break-out from the stellar envelope of the progenitor star of SN2006aj. But, can the detailed broad-band observations of XRF 060218 be reproduced by the CB model?

Amati et al. (2006) showed that XRF 060218 complies with the so-called Amati correlation’ (Amati 2002) for GRBs and XRFs and concluded that it indicates that XRF 060218 *was not* a GRB viewed far off axis. In the CB model, the conclusion is the opposite one ! The observed correlation between peak and isotropic energies of GRBs *and* XRFs is a prediction (Dar & De Rújula 2000, DD2004, Dado, Dar & De Rújula 2007b) trivially following from the kinematics of ICS. The fact that XRF 060218 complies with it corroborates that it *was* a GRB viewed far off axis. In this model, the isotropic equivalent  $\gamma$ -ray energy emission of a typical CB is  $\approx 0.8 \times 10^{44} [\delta_0]^3$  erg (DD2004). Thus, the reported  $E_{\text{iso}} \approx (6.2 \pm 0.3) \times 10^{49}$  erg implies that the CB which generated the dominant peak of XRF 060218 had  $\delta_0 \sim 92$ . It then follows from Eq. (6) that its measured  $E_p = 4.6$  keV implies (for the typical  $T(0) \sim 1$  eV) a Lorentz factor  $\gamma_0 \sim 103$ ,  $\gamma_0 \theta \approx 1.1$  and a viewing angle  $\theta \sim 1.18. \times 10^{-2}$ .

The best sampled light curves of XRF 060218 one is the XRT 0.3-10 keV light curve (Campana et al. 2006b). Thus, first we have fitted the XRT light curve with prompt ICS emission plus SR. We have assumed that the prompt ICS emission was dominated by two pulses - an early pulse plus a main pulse, as suggested by the hardness ratio and BAT light curve. The SR contribution was calculated, using Eqs. (22,26) for a constant density ISM, with  $\gamma_0 \theta = 1.1$ ,  $\beta_X = 1.1$  and a best fit value for the break time. Then, the  $E t^2$  - law for ICS peaks was used to predict the UVOT and BAT light curves. Fig. 10c shows the CB model description of the unabsorbed Swift XRT light curve. Fig. 10d shows the CB model description of the Swift hardness ratio measured with the XRT. Figs. 10e, 10e show the CB model prediction of the Swift dereddened UVOT light curve in the UVW2 filter and the Swift BAT light curve in the 15-150 keV band, respectively, which follow from the  $E t^2$ -law. The afterglow parameters are listed in Table 1. The ICS parameters are listed in Table 2.

We conclude that this XRF060218/SN2006aj pair is in full agreement with the predictions of the CB model. The rich structure of its UVO AG is as expected. Its X-ray light curve has the canonical shape seen in ordinary GRBs. Both of these results are explicitly dependent on the fact that XRFs are GRBs produced by CBs with much smaller Doppler factors, because they are viewed at larger angles or have intrinsically smaller Doppler factors. The data is inconsistent with a black body component produced by a shock break-out through the stellar envelope, or by any other mechanism. The start time of the X-ray emission does not constrain the exact time of the core’s collapse before the launch of the CBs, nor does it constrain possible ejections of other CBs farther off axis, prior<sup>6</sup> to the trigger-time of XRF 060218.

## 6. Conclusions and outlook

The rich data on GRBs gathered after the launch of Swift, as interpreted in the CB model and as we have discussed here and in recent papers (e.g., Dado et al. 2006, 2007, 2008a, 2008b) has taught us several things:

- Two radiation mechanisms, inverse Compton scattering and synchrotron radiation, suffice within the CB model to provide a very simple and accurate description of long-duration GRBs and XRFs and their afterglows at all frequencies and times. Simple as they are, these two mechanisms and the burst environment generate the rich structure of the light curves at all frequencies and times.
- The historical distinction between prompt and afterglow phases is replaced by a physical distinction: the relative dominance of the Compton or synchrotron mechanisms at different, frequency-dependent times.
- The relatively narrow pulses of the  $\gamma$ -ray signal, the somewhat wider prompt flares of X-rays, and the much wider humps sometimes seen at UVOIR frequencies of XRFs, have a common origin. They are generated by inverse Compton scattering.
- The synchrotron emission is part of the prompt emission. It dominates the prompt optical emission in ordinary GRBs, the broad band afterglow in GRBs and XRFs and the late time flares.

---

<sup>6</sup>Interestingly, Swift detected gamma rays from the same direction over a month earlier on January 17, 2006 - <http://grb.sonoma.edu/>

- The early time XRT and UVOT data on XRF060218/SN2006aj are inconsistent with a black body emission from a shock break-out through the stellar envelope. Instead, they support the CB model interpretation of ICS of glory light by a breaking out jet from SN2006aj. The start time of the X-ray emission does not constrain the exact time of the core’s collapse before the launch of the CBs, nor does it constraint possible ejections of other CBs farther off axis.
- Despite its simplicity and approximate nature, the CB model continues to provide extremely successful description of long GRBs and XRFs. Its testable predictions, so far, are in complete agreement with the main established properties of their prompt emission and afterglow at all times and frequencies.

We re-emphasize that the results presented in this paper are based on direct applications of our previously published explicit predictions. Our master formulae, Eq. (12) for ICS and Eqs. (22, 26, 33) for the synchrotron component describe all the data very well. But, could they just be very lucky guesses? The general properties of the data are predictions. But, when fitting cases with many flares, are we not ‘over-parametrizing’ the results? Finally, the  $E t^2$  law plays an important role. Could it be derived in a different theory?

When their collimated radiation points to the observer, GRBs are the brightest sources in the sky. In the context of the CB model and of the simplicity of its underlying physics, GRBs are not persistent mysteries, ‘the biggest of explosions after the Big Bang’, and a constant source of surprises, exceptions and new requirements. Instead, they are well-understood and can be used as cosmological tools, to study the history of the intergalactic medium and of star formation up to large redshifts, and to locate SN explosions at a very early stage. As interpreted in the CB model, GRBs are not ‘standard candles’, their use in ‘Hubble-like’ analyses would require further elaboration. The GRB conundra have been reduced to just one: ‘how does a SN manage to sprout mighty jets?’ The increasingly well-studied ejecta of quasars and microquasars, no doubt also fired in catastrophic accretion episodes on compact central objects, provides observational hints with which, so far, theory and simulations cannot compete.

The CB model underlies a unified theory of high energy astrophysical phenomena. The information gathered in our study of GRBs can be used to understand, also in very simple terms, other phenomena. The most notable is (non-solar) Cosmic Rays. We allege (Dar et al. 1992, Dar & Plaga 1999) that they are simply the charged ISM particles scattered by CBs, in complete analogy with the ICS of light by the same CBs. This results in a successful description of the spectra of all primary cosmic-ray nuclei and electrons at all observed energies (Dar and De Rújula 2006a). The CB model also predicts very simply

the spectrum of the gamma background radiation and explains its directional properties (Dar & De Rújula 2001a,2006b). Other phenomena understood in simple terms include the properties of cooling core clusters (Colafrancesco, Dar & De Rújula 2003) and of intergalactic magnetic fields (Dar & De Rújula 2005). The model may also have a say in ‘astrobiology’ (Dar, Laor & Shaviv 1998, Dar & De Rújula 2001b).

**Acknowledgment:** We would like to thank S. Campana, G. Cusumano, P. Ferrero, D. Grupe, A. D. Kann, K. L. Page, and S. Vaughan, for making available to us the tabulated data of their published X-ray and optical light curves of Swift GRBs. This report is based on a work done in collaboration with A. De Rújula.

## REFERENCES

- Akerlof, C., et al. 1999, *Nature*, 398, 400
- Amati, L., et al. 1999, *NuPhS*, 69, 656
- Amati, L., Frontera, F., Tavani, M., et al. 2002, *A&A*, 390, 81
- Amati, L., 2006, *MNRAS*, 372, 233
- Band, D., et al. 1993, *ApJ*, 413, 281
- Beckmann, V. et al. 2008, *GCN Circ* 7450
- Berger, E. & Gladders, M. 2006, *GCN* 5170
- Berger, E., et al. 2005, *ApJ*, 634, 501
- Bloom, J. S., Frail, D. A. & Kulkarni, S. R. 2003, *ApJ*, 594, 674
- Bloom, J. S. et al. 2008, *arXiv:0803.3215*
- Blustin, A. J. 2007, *Phil. Trans. Royal. Soc. A*, 365, 1263
- Burrows, D. N. & Racusin, J. 2007, *astro-ph/0702633*
- Campana, S., et al. 2006a, *GCN* 5162
- Campana, S., et al. 2006b, *Nature*, 442, 1008
- Cenko, S. B., et al. 2006, *ApJ*, 652, 490
- Colafrancesco, S., Dar, A. & De Rújula, A. 2004, *A&A*, 413, 441
- Colgate, S. A. 1968, *CaJPS*, 46, 476
- Covino, S., et al. 2006, *Il Nuovo Cimento*, (*arXiv: astro-ph/0612643*).
- Covino, S., et al. 2008, *arXiv:0804.4367*
- Cucchiara, A. et al. 2008, *GCN Circ.* 7456
- Curran, P. A., et al. 2006, *arXiv: astro-ph/0610067*
- Cusumano, G., et al. 2006a, *ApJ*. 639, 316
- Cusumano, G., et al. 2006b, *GCN* 4775

- Cwiok, M. et al. 2008, GCN Circ. 7445
- Dado, S. & Dar, A. 2005, *Nuovo Cimento* 120, 731
- Dado, S., Dar, A. & De Rújula, A. 2002a, *A&A*, 388, 1079 (DDD2002a)
- Dado, S., Dar, A. & De Rújula, A. 2003a, *A&A*, 401, 243 (DDD2003a)
- Dado, S., Dar, A. & De Rújula, A. 2003b, *ApJ*, 593, 961 (DDD2003b)
- Dado, S., Dar, A. & De Rújula, A. 2003c, *ApJ*, 594, L89 (DDD2003a)
- Dado, S., Dar, A. & De Rújula, A. 2004, *A&A*, 422, 381 (DDD2004)
- Dado, S., Dar, A. & De Rújula, A. 2006, *ApJ*, 646, L21 (DDD2006)
- Dado, S., Dar, A. & De Rújula, A. 2007a, *ApJ*, 663, 400 (DDD2007a)
- Dado, S., Dar, A. & De Rújula, A. 2007b, arXiv: astro-ph/0701294 (DDD200b)
- Dado, S., Dar, A. & De Rújula, A. 2007c, arXiv: arXiv:0706.0880
- Dado, S., Dar, A. & De Rújula, A. 2008a, *ApJ*, 681, 1408 (DDD2008a)
- Dado, S., Dar, A. & De Rújula, A. 2008b, *ApJ*, 680, 517 (DDD2003b)
- Dai, X., et al. 2007, *ApJ*, 658, 509
- Dai, X., et al. 2008, *ApJ*, 682L, 77
- Dar, A. 1998, *ApJ*, 500, L93
- Dar, A. 2006, *ChJAS*, 6, 301
- Dar, A. & Plaga, R. 1999, *A&A*, 349, 259
- Dar, A. & De Rújula, A. 2000a, arXiv: astro-ph/0008474
- Dar, A. & De Rújula, A. 2000b, arXiv: astro-ph/0012227
- Dar, A. & De Rújula, A. 2001a, *MNRAS*, 323, 391
- Dar, A. & De Rújula, A. 2001b, *Astrophysics and Gamma Ray Physics in Space* (eds. A. Morselli and P. Picozza), Frascati Physics Series Vol. XXIV pp. 513-523 (arXiv: astro-ph/0110162)
- Dar, A. & De Rújula, A. 2004, *Physics Reports*, 405, 203 (DD2004)

- Dar, A. & De Rújula, A. 2005, PRD, 72, 123002
- Dar, A. & De Rújula, A. 2006, arXiv: hep-ph/0606199 (Physics Reports 2008, in press)
- Dar, A., Laor, A. & Shaviv, N. J. 1998, PRL, 80, 5813
- Dar, A. & Plaga, R. 1999, A&A, 349, 259
- Della Valle, M., et al. 2006, Nature 444, 1050
- De Rújula, A. 1987, Phys. Lett. 193, 514
- De Rújula, A. 2007a , arXiv:0707.0283
- De Rújula, A. 2007b, arXiv:0711.0970 (in press)
- De Rújula, A. 2007b, arXiv:0801.0397
- Evans, P. A., et al. 2007, A&A, 469, 379
- Fenimore, E. E., et al. 1995, ApJ, 448, L101
- Ferrero, P., et al. 2006, A&A, 457, 857
- Ferrero, P. et al. 2008, arXiv:0804.2457
- Frederiksen, J. T. et al. 2003, arXiv: astro-ph/0303360
- Frederiksen, J.T., et al. 2004, Astrophys. J. 608, L13
- French, J., & Jelinek, M. 2006, GCN 5165
- Frail, D. A., et al. 2001, ApJ, 562, L55
- Galama, T. J. et al. 1998a, ApJ, 497, L13
- Galama, T. J. et al. 1998b, Nature, 395, 670
- Gal-Yam, A., et al. 2006, Nature, 444, 1053
- Ghisellini, G., Celotti, A., & Lazzati, D. 2000, MNRAS, 316, L5
- Gomboc, A., et al. 2008, arXiv0804.1727
- Golenetskii, S. et al. 2008, GCN Circ. 7482
- Guenther, E. W., et al. 2006, GCN 4863

- Heise, J., et al. 2001, *Gamma-Ray Bursts in the Afterglow Era*, (Eds. E. Costa, F. Frontera, and J. Hjorth) Springer-Verlag, p. 16
- Hjorth, J., et al. 2003, *Nature*, 423, 847
- Huang, K. Y., et al. 2007, *ApJ*, 654, L25
- Jakobsson, P., et al. 2006, *A&A*, 460, L13
- Karpov, S. et al. 2008, *GCN Circ.* 7558
- Khamitov, I. M., et al. 2007, *AstL*, 33, 797
- Kocevski, D., Ryde, F. & Liang, E., 2003, *ApJ*, 596, 389
- Krimm, H., et al. 2005, *GCN Circ.* 3117
- Kumar, P., et al. 2007, *MNRAS*, 376, L57
- Li, W., et al. 2003, *ApJ*, 586, L9
- Liang E. W., et al. 2007, *ApJ*, 653, L81
- Liang, E. W., et al. 2008, *ApJ*, 675, L528
- Lipkin, Y. M., et al. 2004, *ApJ*, 606, 381
- Malesani, D., et al. 2003, *ApJ*, 609, L5
- Malesani, D. et al. 2004, *ApJ*, 609, L5
- Malesani, D., et al. 2008, *arXiv:0805.1188*
- Mangano, V., et al. 2007, *A&A*, 470, 105
- Marshall, G., et al. 2006, *GCN*, 4792
- Mazzali, P. A., et al. 2006, *ApJ*, 645, 1323
- McGlynn, S., et al. 2007, *arXiv: astro-ph/0702738*
- Mészáros, P. 2002, *ARA&A*, 40, 137
- Mészáros, P. 2006, *Rept. Prog. Phys.* 69, 2259
- Mirabal, N. & Halpern, J. P., 2006, *GCN* 4709

- Mirabal, L., et al. 2006, ApJ, 643, L99
- Mirabel, I.F. & Rodriguez, L.F. 1999 ARA&A, 37, 409.
- Modjaz, M., et al. 2008, arXiv:0805.2201
- Molinari, E., et al. 2007, A&A, 469, L13
- Monfardini, A., et al. 2006, ApJ, 648, 1125
- Nisenson, P. & Papaliolios, C. 2001, ApJ, 548, L201
- Nishikawa, K.-I. et al. 2003, ApJ, 595, 555
- Nousek, J., et al. 2006, ApJ, 642, 389
- Nysewander, M., et al. 2007, arXiv:0708.3444
- O’Brien, P. T., et al. 2006, ApJ, 647, 1213
- Page, K. L. et al. 2007, ApJ, 663, 1125
- Panaitescu, A., et al. 2006, MNRAS, 369, 2059
- Parsons, A., et al. 2006, GCN 5370
- Perley, D. A., et al. 2008, ApJ, 672, 449
- Pian, E., et al. 2006, Nature, 442, 1011
- Piran, T. 1999, Physics Reports, 314, 575
- Piran, T. 2000, Physics Reports, 333, 529
- Piran, T. 2005, RMP, 76, 1143
- Piro, L., et al. 1998, A&A, 331, L41
- Piro, L., et al. 2000, Science, 290, 955
- Quimby, R. M., et al. 2006, ApJ, 640, 402
- Quimby, R. M., et al. 2006b, GCN Circ. 5366
- Racusin, J. L. et al. 2008a, arXiv:0801.4749
- Racusin, J. L. et al. 2008b, GCN Circ. 7427

- Racusin, J. L. et al. 2008, GCN Circ. 7459
- Reeves, J. N., et al. 2002, Nature, 416, 512
- Rhoads, J. E. 1997, ApJ, 487, L1
- Rhoads, J. E. 1999, ApJ, 525, 737
- Rodriguez, L.F. & Mirabel, I.F. 1998, New Astron. Rev. 42, 649.
- Romano, P., et al. 2006, A&A 450, 59
- Rykoff, E. S., et al. 2004, 2004, ApJ, 601, 1013
- Salamanca, I. et al. 1998, MNRAS, 300, L17S
- Salamanca, I., Terlevich, R. J. & Tenorio-Tagle, G. 2002, MNRAS, 330, 844
- Sari, R., Piran, T. & Halpern, J. P. 1999, ApJ, 519, L17
- Sato, G., et al. 2007, ApJ 657, 359
- Schaefer, B. E. 2006, arXiv: astro-ph/0612285 ???
- Shaviv, N. J. & Dar, A. 1995, ApJ, 447, 863
- Sollerman et al. 2006, A&A, 454, 503
- Soderberg, A. M., et al. 2006, Nature, 442, 1014
- Stanek, K. Z., et al. 2003, ApJ, 591, L17
- Stanek, K. Z., et al. 2007, ApJ, 654 L21
- Theone, C. C., et al. 2006, GCN 5373
- Turatto, M., et al. 2000, ApJ, 534, L57
- Vaughan, S., et al. 2006, ApJ, 638, 920
- Vestrand, J. A. et al. 2006, Nature, 442, 172.
- Vreeswijk, P. M. et al. 2008, GCN Circ. 7444
- Yonetoku, D., et al. 2004, ApJ. 609, 935
- Watson, D., et al. 2003, ApJ, 595, L29

- Waxman, E. 2003a, *Lect. Notes Phys.* 598, 393
- Waxman, E., Meszaros, P. & Campana, S. 2007, *ApJ*, 667, 351
- Wigger, C., et al. 2004, *ApJ*, 613, 1088
- Wigger, C., et al. 2008, *ApJ*, 675, 553
- Willis, D. R., et al. 2005, *A&A*, 439, 245
- Wozniak, P. R., et al. 2005, *ApJ*, 627, L13
- Wozniak, P. R., et al. 2006, *ApJ*, 642, L99
- Wozniak, P., et al. 2008, *GCN Circ.* 7464
- Yoshida, A., et al. 1999, *A&AS*, 138, 433
- Yoshida, A., et al. 2001, *ApJ*, 557, L27
- Wu, B. & Fenimore, E. 2000, *ApJ*, 535, L29
- Zhang, B. & Mészáros, P. 2004, *IJMPA*, 19, 2385
- Zhang, B. 2007, *ChjAA*, 7, 1
- Zhang, Bin-Bin., Liang, E. & Zhang, B. 2008, *GCN Circ.* 7511
- Ziaeeepour, H., et al. 2008, *MNRAS*, 385, 453

Table 1. CB model afterglow parameters

GRB/XRF	$t_0[s]$	$\theta \gamma_0$	$p$
060729	(606)	(2.52)	2.20
061121	248	1.42	2.20
050315	12362	0.965	2.20
061007	40	$\ll 1$	2.20
061126	142	1.08	1.84
080319B	72	( $\ll 1$ )	2.16
060211A	64596	0.54	2.11
061110A	29402	0.81	2.04
080307	28893	1.00	2.13
051021B	13092	0.82	2.24
080303	15196	0.79	2.15
070220	1314	0.64	2.16
060526	1840	0.93	2.20
060206	2570	1.035	2.20
050820A	2692	1.128	2.22
060418	$< 60$	1.73	2.20
07010A	857	1.21	1.92
050318	273	1.61	2.19
050326	379	1.28	2.16
051008	1233	1.17	2.20
050814	7737	1.14	2.18
061019	194	2.22	2.20
070306	1437	1.91	2.20
060813	273	1.60	2.20
070521	551	1.33	2.23
080207	95	0.98	1.87
060807	9867	1.02	2.21
070419B	1146	0.99	2.20
070420	60	2.00	2.22
050319	73	0.92	2.20
	999	2.05	2.22

Table 1—Continued

GRB/XRF	$t_0[s]$	$\theta \gamma_0$	$p$
060605	(< 1000)	(1.00)	2.20
060607A	(54)	(1.07)	2.20
060218	267	1.10	1.94

Table 2. Time parameters of the last two major X-flares

GRB/XRF	Band	$t_1$ [s]	$\Delta t_1$ [s]	$t_2$ [s]	$\Delta t_2$ [s]
060729	X	122	6.2	153	19.1 s
061121	X	52	12.4	97	18.8
050315	X	-5	6.9	16.4	5.4
061007	X	23	5.5		
061126	X	4.4	7.8		
080319	X	37	5.0		
060211A	X	79	30		
061110A	X	35	54		
080307	X	0	373		
051021B	X	0	67		
080303	X	0	114		
070220	X	0	75		
060526	X	233	16.4	272	31.6
060206	X	581	43.2	4187	549
050820A	X	205	29	2173	2225
060418	X	60	12	118	9.8
07010A	X	18990	30968		
050814	X			0	2074
070306	X	154	20	364	50
060813	X	37	58	0	246
070521	X	0	222		
060807	X	0	26		4635
070419B	X	106	41	134	87
070420	X	0	54		
050319	X	0	54	2003	
060605	X	0	83	67	154
060607A	X				
060218	X	0	950	0	



Table 3. Peak flux density (PFD) of XRF 060218 in the Swift UVOT filters, corrected for Galactic reddening  $E(B-V)=0.14$ , and their constant value calculated from the XRT unabsorbed peak energy flux (PEF) in the 0.3-10 keV band, using the ‘ $E t^2$  law’

Filter	$\lambda$ [nm]	E(center) [eV]	FWHM	Observed PED [erg cm <sup>-2</sup> s <sup>-1</sup> ]	PFD [ $\mu$ Jansky]	CB Model [ $\mu$ Jansky]
UVW2	188	6.60	76 nm	$(2.29 \pm 0.23) \times 10^{-12}$	$355 \pm 36$	$374 \pm 135$
UVM1	217	5.71	51 nm	$(1.30 \pm 0.10) \times 10^{-12}$	$399 \pm 31$	$374 \pm 135$
UVW1	251	4.94	70 nm	$(1.17 \pm 0.12) \times 10^{-12}$	$352 \pm 37$	$374 \pm 135$
U	345	3.55	88 nm	$(8.89 \pm 0.85) \times 10^{-13}$	$406 \pm 44$	$374 \pm 135$
B	439	2.83	98 nm	$(5.99 \pm 0.56) \times 10^{-13}$	$393 \pm 37$	$374 \pm 135$
V	544	2.28	75 nm	$(2.59 \pm 0.10) \times 10^{-13}$	$340 \pm 34$	$374 \pm 135$

Table 4. Peak times of the energy flux of XRF 060218 in the Swift XRT and UVOT filters and their expected values from the  $E t^2$  law

Band	E(eff) [eV]	Observed $t_{peak}$ [s]	CB Model $t_{peak}$ [s]
X	5150	$985 \pm 50$	$985 \pm 50$
X	3000	$1310 \pm 90$	$1290 \pm 65$
X	600	$2790 \pm 2550$	$2770 \pm 150$
UVW2	6.60	$25,800 \pm 5,000$	$27,500 \pm 1,400$
UVM1	5.71	$36,208 \pm 8,000$	$29,600 \pm 1,800$
UVW1	4.94	$41,984 \pm 10,000$	$32,000 \pm 1,600$
U	3.59	$42,864 \pm 10,000$	$37,500 \pm 1,900$
B	2.82	$39,600 \pm 15,000$	$42,000 \pm 2,100$
V	2.28	$47,776 \pm 10,000$	$47,000 \pm 2,400$

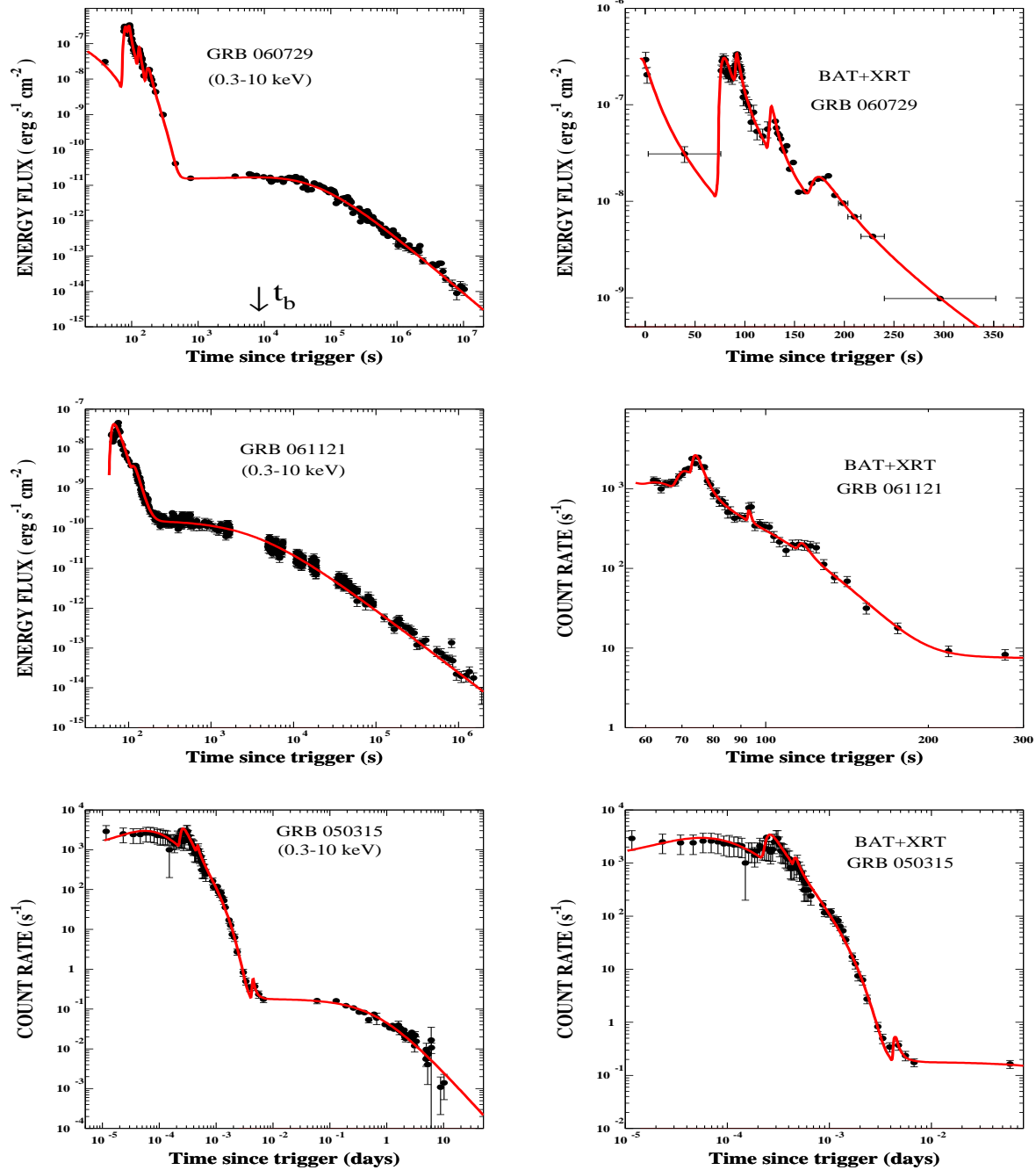


Fig. 1.— Comparison between Swift observations of GRB canonical X-ray light-curves and their CB model description. **Top left (a):** Comparisons between the X-ray light-curve of GRB 060729 and its CB model description. **Top right (b):** Enlarged view of the comparison between the X-ray light-curve of GRB 060729 at early time. **Middle left (c):** Comparisons between the X-ray light-curve of GRB 061121 and its CB model description. **Middle right (d):** Enlarged view of the comparison between the X-ray light-curve of GRB 061121 and its CB model description at early time. **Bottom left (e):** Comparison between the X-ray light-curve of GRB 050319 and its CB model description. **Bottom right (f):** Enlarged view of the comparison between the X-ray light-curve of GRB 050319 and its CB model description at early time.

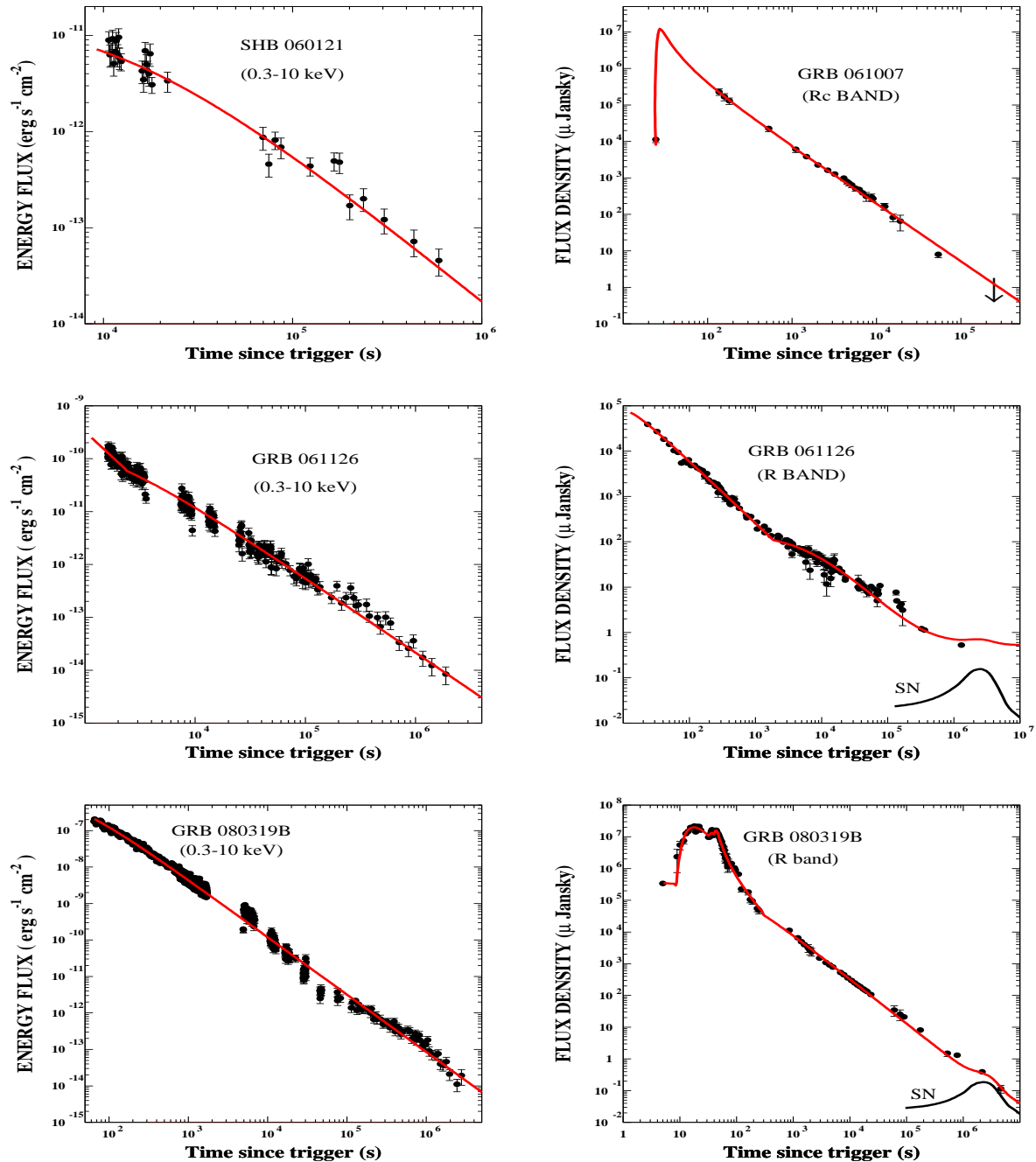


Fig. 2.— Comparison between broad-band observations of GRBs with single-power-law decaying AGs and their CB model descriptions. **Top left (a):** Comparisons between the X-ray light curve of GRB 061007 and its CB model description. **Top right (b):** Comparisons between the R-band light-curve of GRB 061007 and its CB model description. **Middle left (c):** Comparisons between the X-ray light-curve of GRB 061126 and its CB model description. **Middle right (d):** Comparisons between the R-band light-curve of 061126 and its CB model description. **Bottom left (e):** Comparisons between the X-ray light-curve of GRB 080319B and its CB model description. **Bottom right (f):** Comparisons between the R-band light-curve of GRB 080319B and its CB model description.

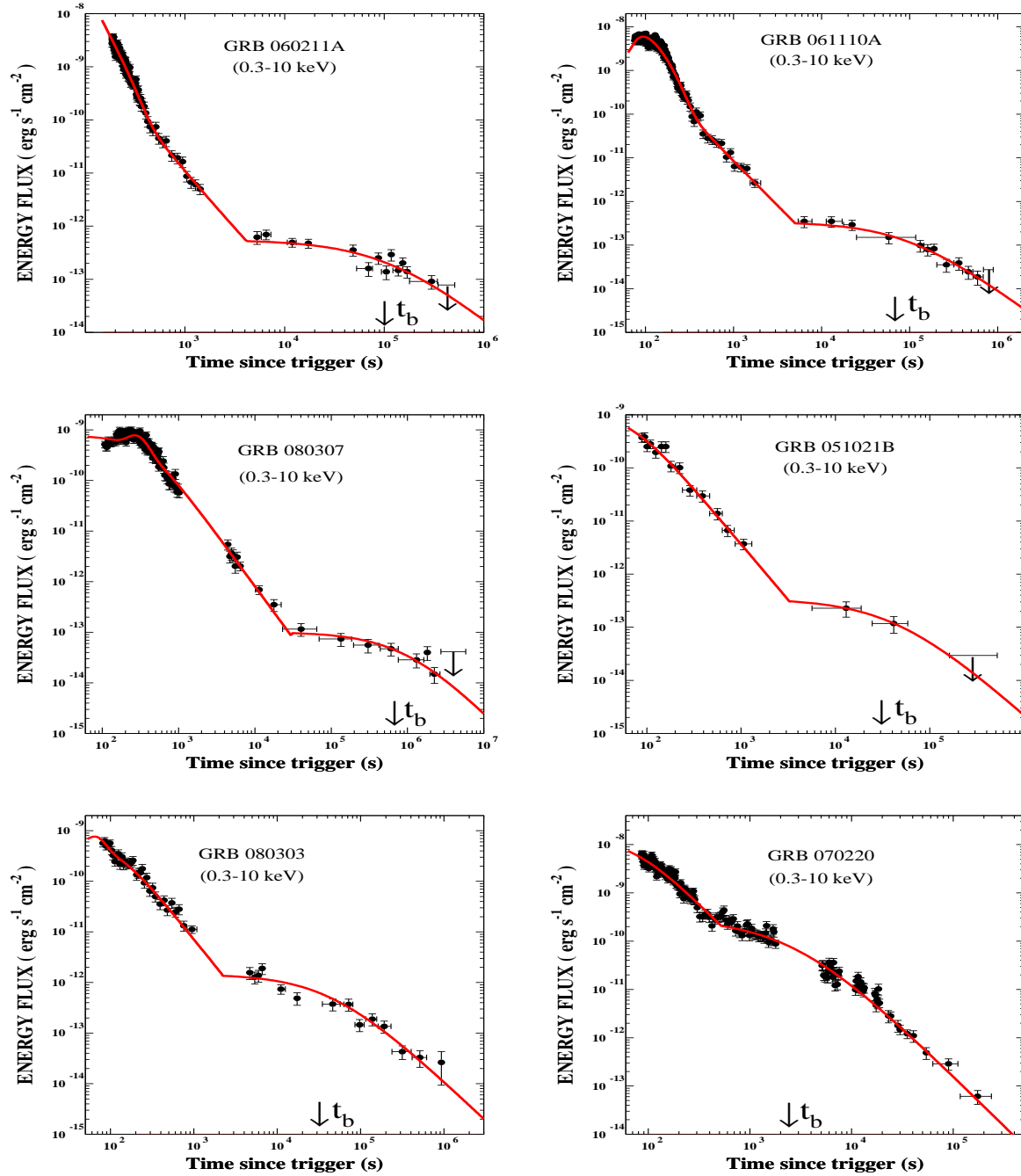


Fig. 3.— Comparison between semi canonical X-ray light curves of Swift GRBs (Evans et al. 2007) and their CB model description: **Top left (a):** GRB 051021B . **Top right (b):** GRB 060211A. **Middle left (c):** GRB 061110A. **Middle right (d):** GRB 070220. **Bottom left (e):** GRB 080303. **Bottom right (f):** GRB 080307.

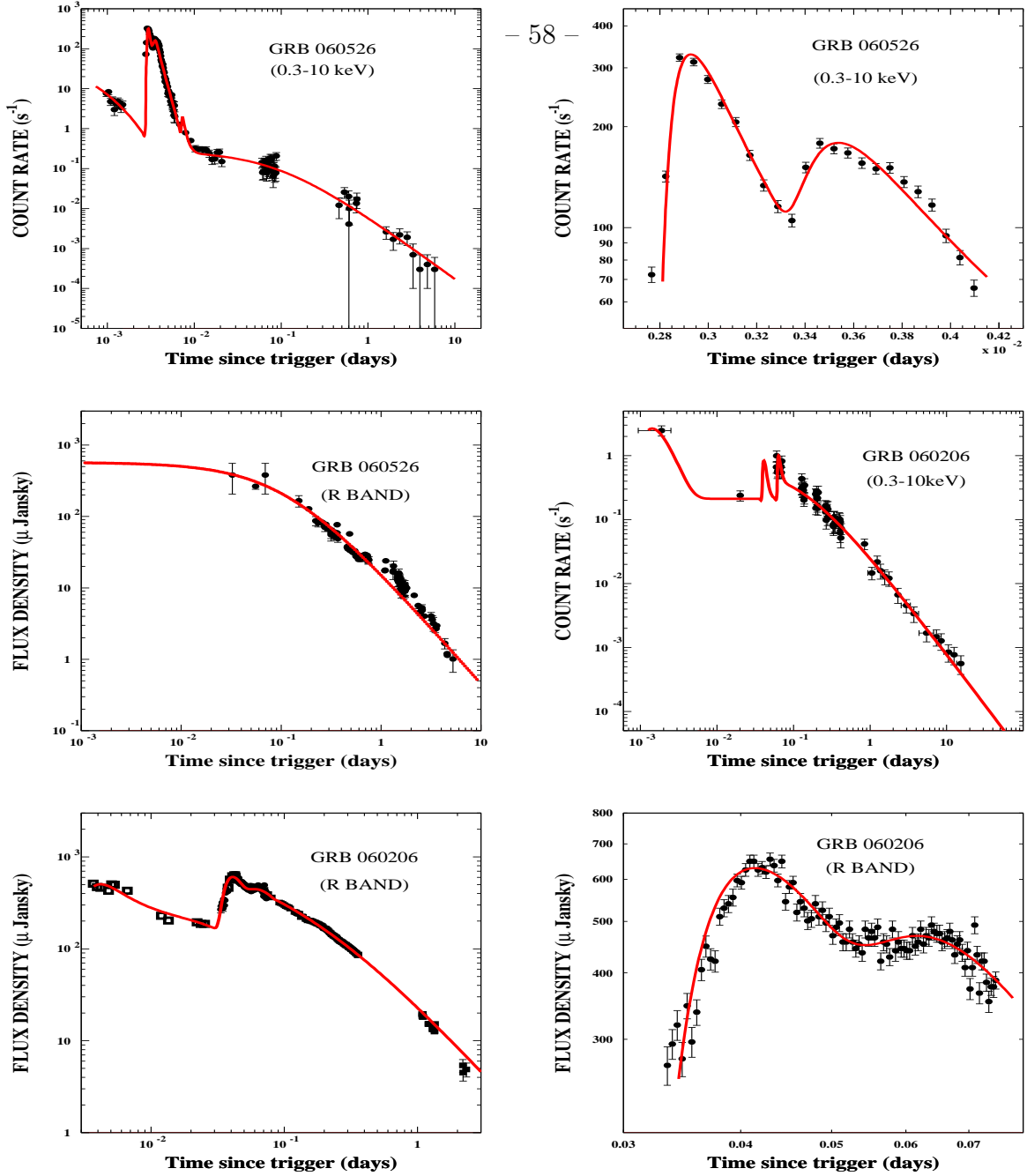


Fig. 4.— Comparison between broad-band observations of GRBs with chromatic early-time afterglow and their CB model descriptions. **Top left (a):** Comparisons between the XRT light-curve of GRB 060526 and its CB model description. **Top right (b):** Comparisons between the early X-ray giant flares of GRB 60526 and their CB model description as ICS flares. **Middle left (c):** Comparisons between the R-band light-curve of GRB 060526 and its CB model description. **Middle right (d):** Comparisons between the XRT light-curve of GRB 060206 and its CB model description. **Bottom left (e):** Comparisons between the R-band light-curve of GRB 060206 (Wozniak et al. 2006, Stanek et al. 2007 and Monfardini et al. 2006) and its CB model description. The CB model light curve was calculated with the parameters of the X-ray light curve. **Bottom right (f):** Enlarged view of two early time R-band synchrotron flares and their CB model description.

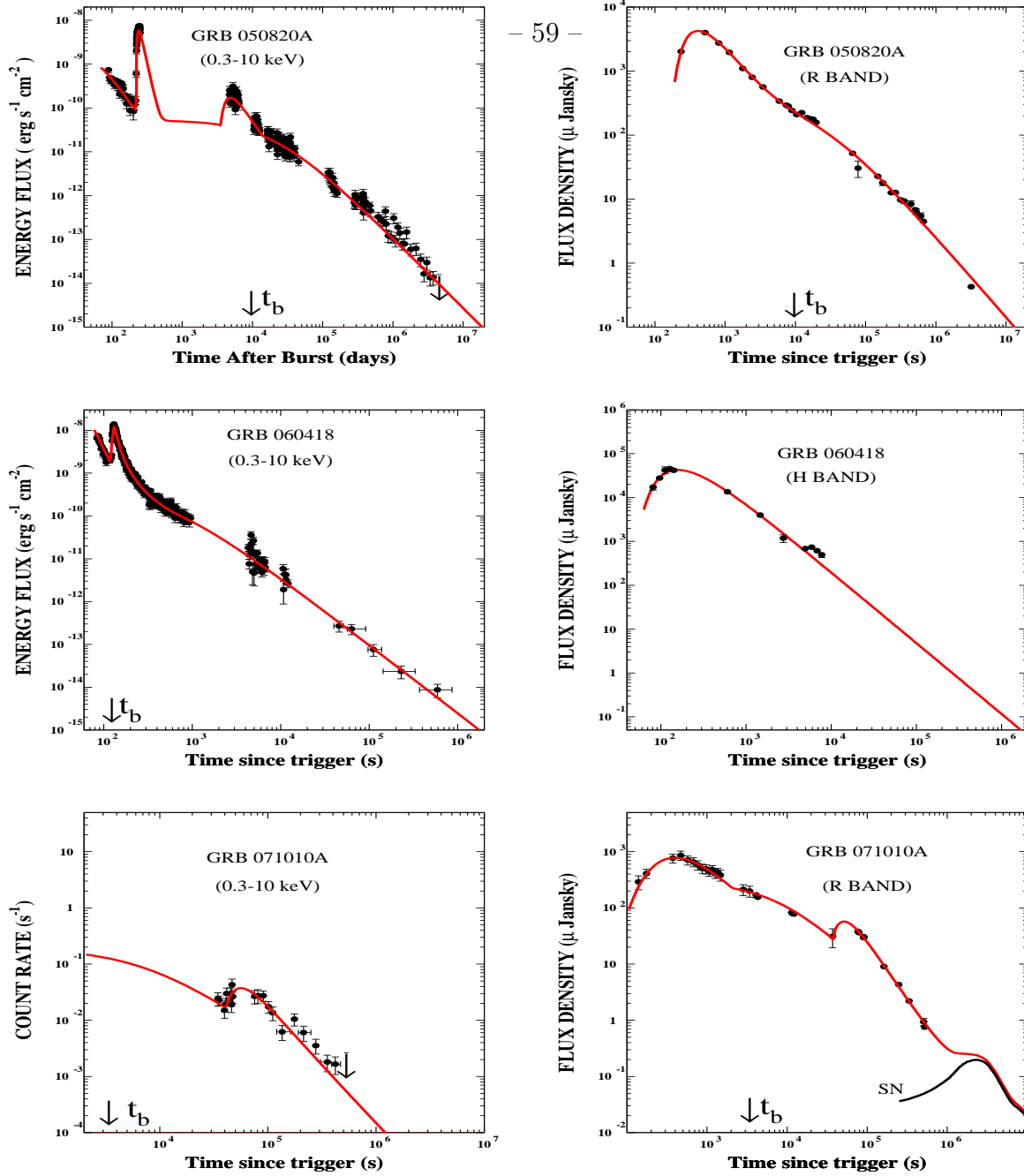


Fig. 5.— Comparison between broad-band observations of GRBs with chromatic early-time afterglow and their CB model descriptions. **Top left (a):** Comparisons between the X-ray light curve of GRB 050820A and its CB model description. **Top right (b):** Comparisons between the R-band light-curve of GRB 050820A and its CB model description. **Middle left (c):** Comparisons between the X-ray light-curve of GRB 060418 and its CB model description. **Middle right (d):** Comparisons between the H-band light-curve of 060418 and its CB model description. **Bottom left (e):** Comparisons between the X-ray light-curve of GRB 071010A and its CB model description. **Bottom right (f):** Comparisons between the R-band light-curve of GRB 07101A and its CB model description.

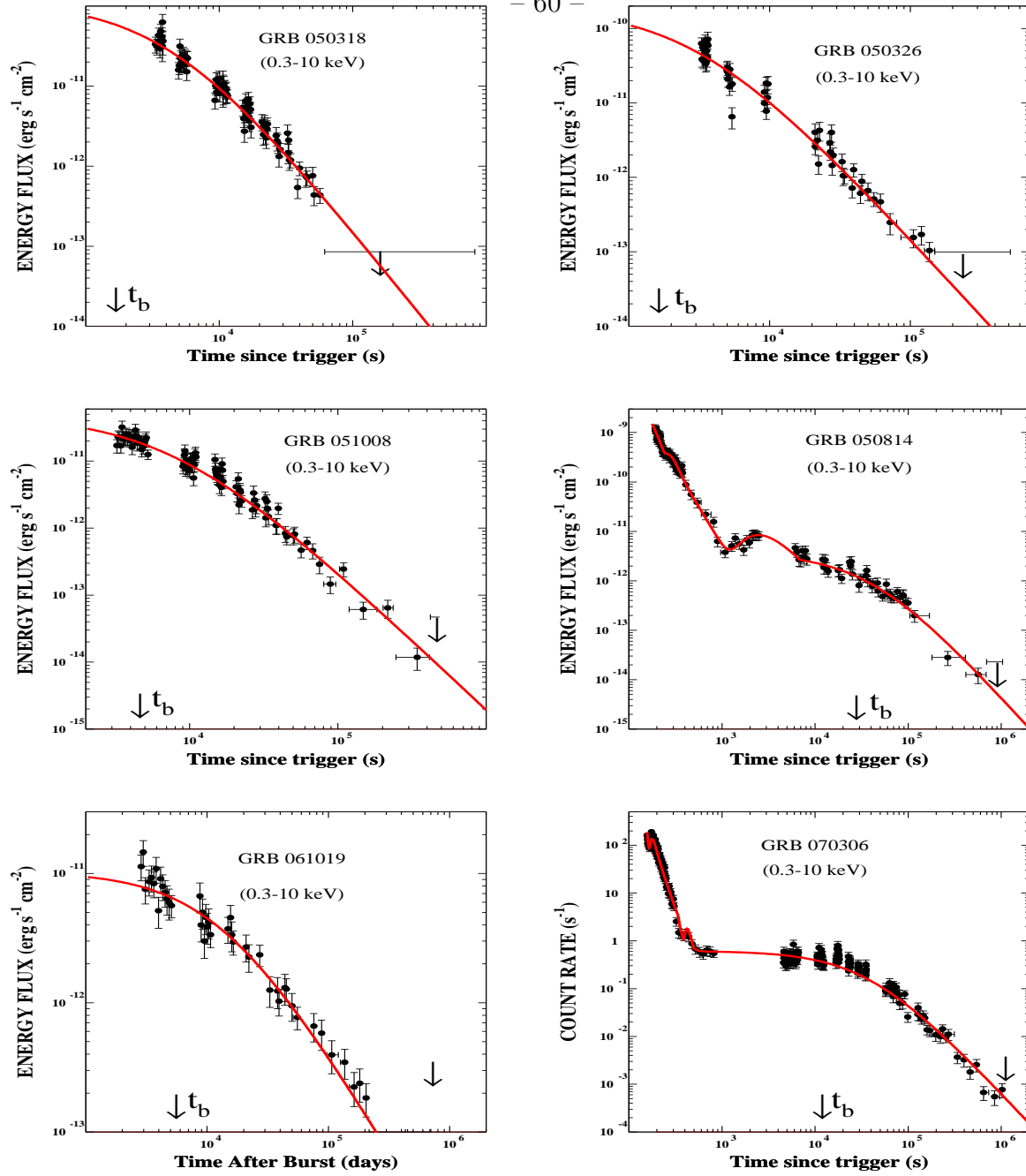


Fig. 6.— Comparison between XRT-light curves of Swift GRBs (Evans et al. 2007) with late time decay index  $\alpha > 2$  and their CB model descriptions assuming an isothermal-sphere density profile  $n = n_0/(1 + (r/r_c)^2)$ : **Top left (a)**: GRB 050318 and its CB model description. **Top right (b)**: GRB 050326 and its CB model description. **Middle left (c)**: GRB 051008 and its CB model description. **Middle right (d)**: GRB 050814 and its CB model description. **Bottom left (e)**: GRB 061019 and its CB model description. **Bottom right (f)**: GRB 070306 and its CB model description.

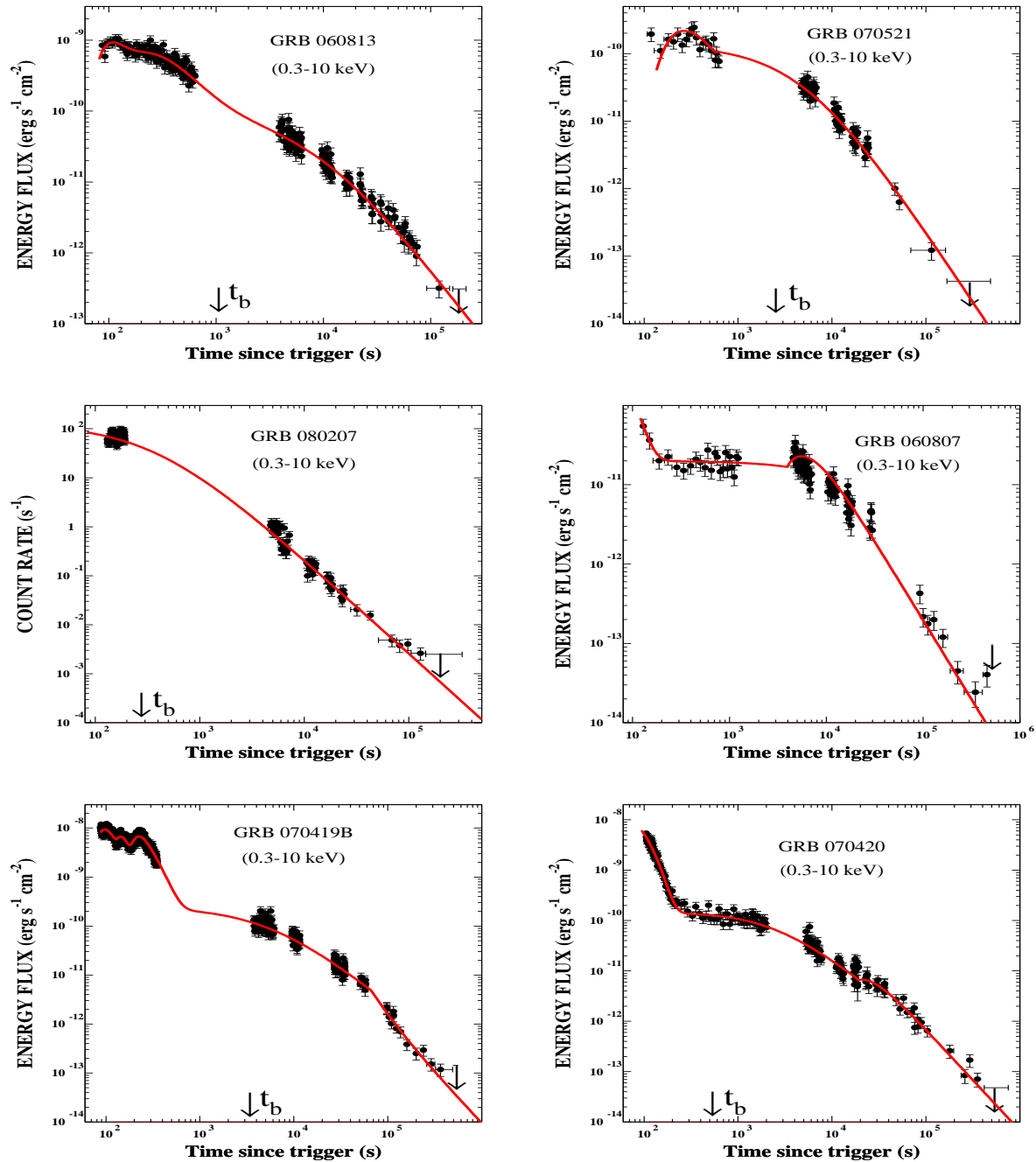


Fig. 7.— Comparison between the Swift XRT-light curves (Evans et al. 2007) with late-time decay index  $\alpha > 2$  or a late-time flare and their CB model description: **Top left (a)**: GRB 060813 with a steep late-time decay. **Top right (b)**: GRB 070521 with a steep late-time decay. **Middle left (c)**: GRB 080207 with a steep late-time decay. **Middle right (d)**: GRB 060807 with a late-time flare. **Bottom left (e)**: GRB 070419B with a late-time flare. **Bottom right (f)**: GRB 070420 with a late-time flare.

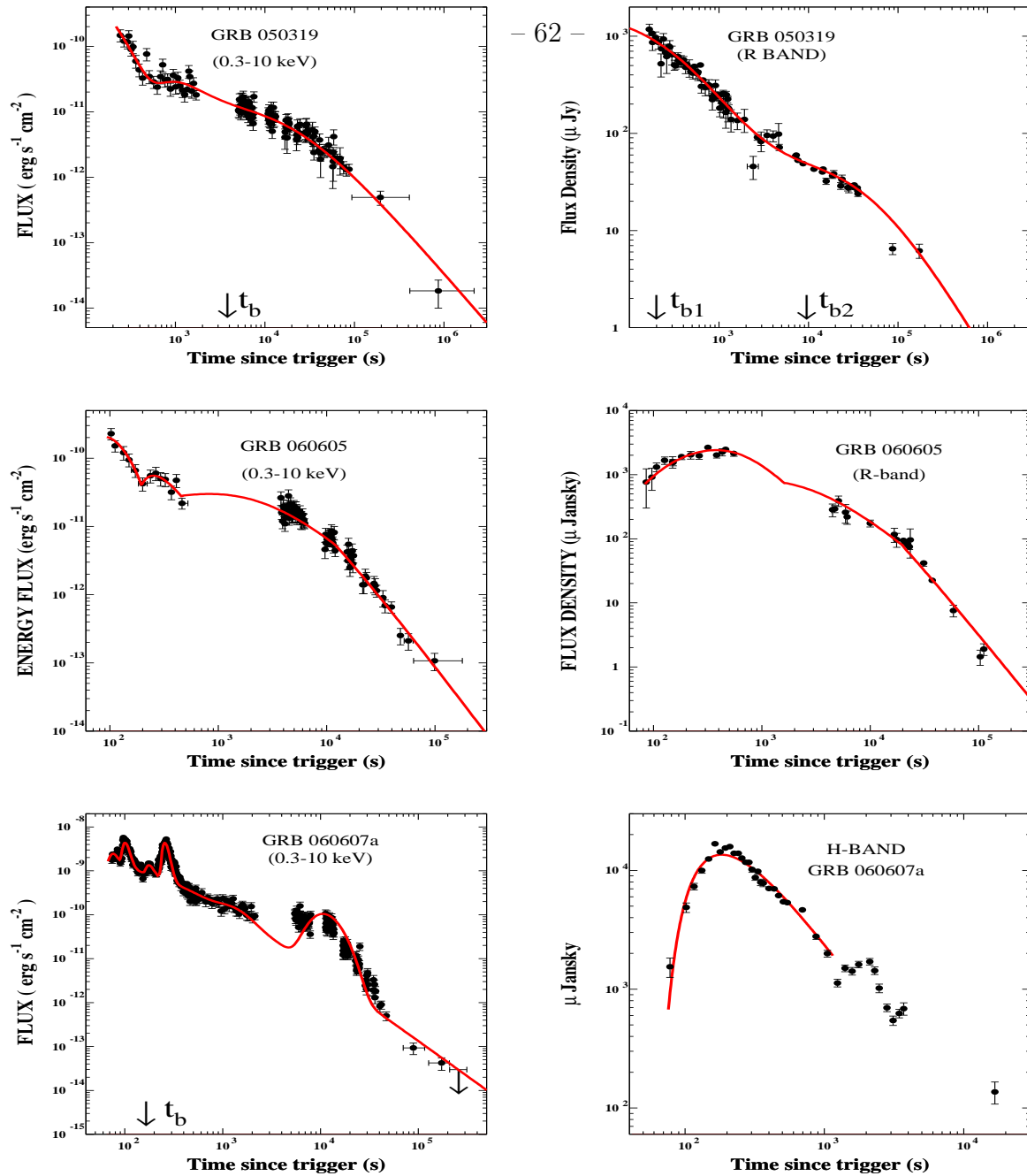


Fig. 8.— Comparison between complex chromatic light curves of GRBs and their CB model description. **Top left (a):** The X-ray light curve of 050319A as measured with the Swift XRT (Cusumano et al. 2005) and its CB model description. **Top right (b):** The optical R-band light curve (Wozniak et al. 2005, Huang et al. 2006 and references therein) of GRB 050319 and its CB model description based on the CB model fit to its X-ray light curve. **Middle left (c):** The X-band light-curve of GRB 060605 and its canonical CB model description. **Middle right (d):** The  $R_c$ -band light-curve of GRB 060605 (Ferrero et al. 2008) and the CB model prediction based on the CB model description of its X-ray light curve. The early rise corresponds to the early X-ray flare superimposed on the early X-ray plateau phase. **Bottom left (e):** The X-ray light-curve of GRB 060607A and its CB model description. **Bottom right (f):** The H-band light-curve of 060607 (Molinari et al. 2007) and its CB model description based on the CB model fit to its X-ray light curve.

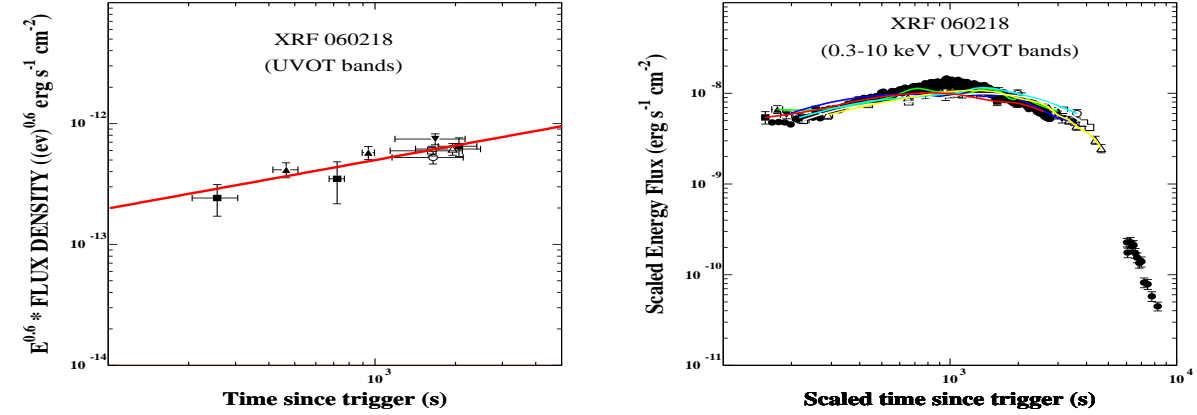
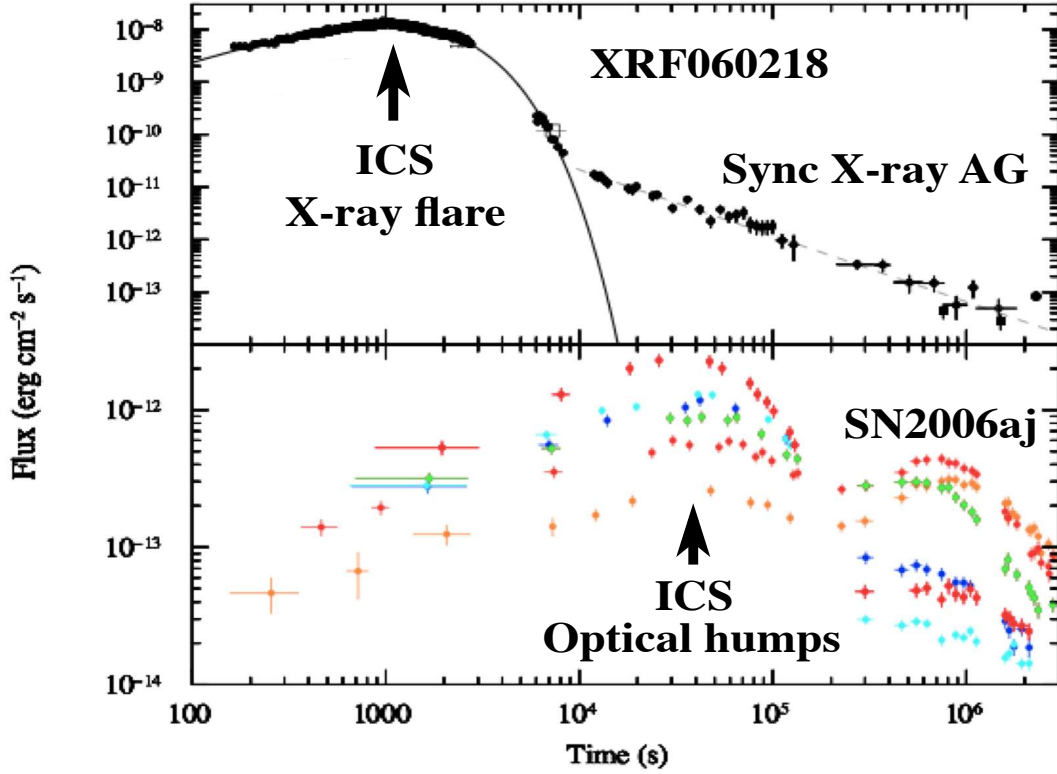


Fig. 9.— X-ray and UVO light curves of XRF 060218/SN2006aj. **Top (a)**: The unabsorbed 0.3-10 keV Swift-XRT light curve. The black line is a sum of a cut-off power-law flux and a black body flux with time-dependent amplitude and temperature adjusted to fit the data (Campana et al. 2006b). The dashed line is their best fit power-law decline beyond 10 ks. The thick arrow indicates the peak-flux time. **Middle (b)**: The energy fluxes corrected for Galactic reddening  $E(B-V)=0.14$  (Campana et al. 2006b) in the UVOT filters: red - V (centered at 544 nm); green - B (439 nm); blue - U (345 nm), light blue - UVW1 (251 nm); magenta - UVM1 (217 nm) and yellow - UVW2 (188 nm), with peak time (roughly indicated by an arrow) which increases with wave length. After 2 days the light curves are overtaken by the light from SN2006aj, which peaks around 10 days after the BAT trigger. **Bottom left (c)**: The energy flux densities in the Swift UVOT filters at  $t < 5$  ks, corrected for Galactic  $E(B-V)=0.14$  reddening and multiplied by  $\nu^{0.6}$ . They are predicted to lie on the plotted universal line,  $A t^{0.4}$ , predicted by the CB model (Eq. 33) for the early time SR contribution. **Bottom right (d)**: Comparison between the unabsorbed XRT energy flux in the 0.3-10 keV band and the energy fluxes measured in the UVOT filters, dereddened by the Galactic  $E(B-V) = 0.14$  (Campana et al. 2006b) and divided by the black body flux.

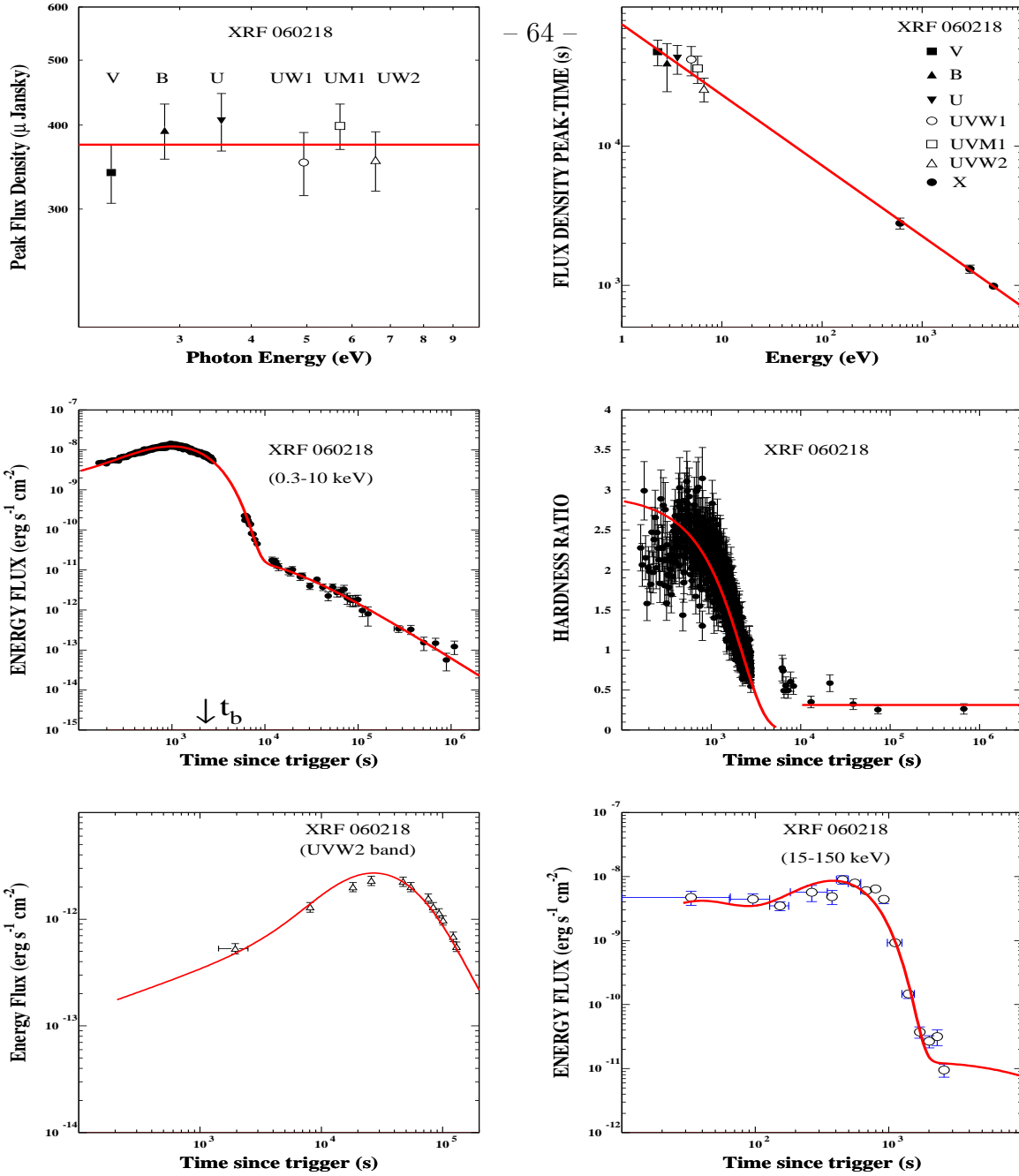


Fig. 10.— Comparison between the broad band observations of XRF 060218 and CB model predictions. **Top left (a)**: The peak energy-flux densities as measured with the UVOT filters corrected for Galactic reddening  $E(B-V)=0.14$  (Campana et al. 2006b), divided by  $E \Delta\lambda/\lambda$  and plotted at the central energies of the UVOT bands. The line is their constant value expected from the  $E t^2$  law. **Top right (b)**: Comparison between the peak time of the energy flux in the Swift’s XRT and UVOT filters (Table 4) and the  $E t^2$  law (red line). **Middle left (c)**: The Swift unabsorbed XRT light curve (Campana et al. 2006b), and its CB model description. The ICS of glory light at early time, is taken over by SR around 9 ks. **Middle right (d)**: The Swift hardness ratio in the XRT energy band (Evans et al 2007) and the CB model prediction for an early time ICS taken by SR around 9 ks. **Bottom left (e)**: Comparison between the Swift UVOT light measured with the UVW2 filter and corrected for Galactic extinction (Campana et al. 2006b), before being overtaken by the light from SN2006aj, and its CB model description. See the text for details. **Bottom Right (f)**: Comparison between the BAT  $\gamma$ -ray light curve in the 30-150 keV band and its expected shape from the  $E t^2$  law. Deviation are expected for  $E \gtrsim E_p$ . An early peak, hinted by the